Towards a Robust Life Cycle Assessment Tool for Sustainable Pavement Designs: Quantifying Context-Specific Impacts of Pavement Albedo

by

Xin Xu

B.Eng. Civil Engineering, Southeast University, 2011
S.M. Civil and Environmental Engineering, Massachusetts Institute of Technology, 2013

Submitted to the Department of Civil and Environmental Engineering in partial
fulfillment of the requirements for the degree of

Doctor of Philosophy in Civil and Environmental Engineering

at the

Massachusetts Institute of Technology

June 2018

Signature redacted

Author..
Department of Civil and Environmental Engineering
March 31, 2018

Signature redacted

Certified by...
Franz-Josef Ulm
Professor of Civil and Environmental Engineering
Thesis Supervisor

Signature redacted

Certified by...
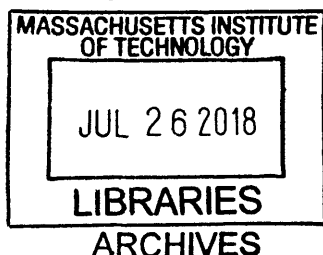Randolph E. Kirchain
Principal Research Scientist, Materials Processing Center
Thesis Co-advisor

Signature redacted

Certified by...
Colette L. Heald
Professor of Civil and Environmental Engineering
Thesis Committee Chair

Signature redacted

Accepted by....................   ....
Jesse H. Kroll
Professor of Civil and Environmental Engineering
Chair, Graduate Program Committee

Towards a Robust Life-Cycle Assessment Tool for Sustainable Pavement Designs: Quantifying Context-Specific Impacts of Pavement Albedo

by
Xin Xu

Submitted to the Department of Civil and Environmental Engineering
on March 31, 2018 in partial fulfillment of
the requirements for the degree of
Doctor of Philosophy in Civil and Environmental Engineering

ABSTRACT

While guidance have been developed for pavement life cycle assessment (LCA) in recent decades, it has not been widely implemented for supporting environmentally conscious pavement designs, partially due to the limitations in sub-models for quantifying the use phase impacts, such as albedo. High-albedo surfaces reflect more shortwave radiation, exerting "radiative forcing" (RF) on the earth. It also affects the ambient temperature and results in changes in building energy demand (BED).

In the past, the impacts of pavement albedo were often ignored or quantified using very simple models. The net effect of RF and BED impacts in the context of pavement LCA remains unknown. This thesis presents a comprehensive approach to assess the effectiveness of pavement albedo modification strategies in urban neighborhoods. To estimate RF impact, we adapt an empirical analytical model from the literature and further incorporate the effects of cloudiness and shadings in the urban area. For BED, we develop a hybrid framework coupling multiple numerical models to account for the interactions between buildings and surrounding environment. Statistical meta-models are employed to facilitate more efficient computations with fewer input variables. The impact of several context-specific factors are taken into account in these models. Case studies are carried out to demonstrate the approach and results for urban neighborhoods in Boston and Phoenix, making use of data extracted from climate simulations and GIS datasets.

Comparative analysis shows that the impact of changing pavement albedo can vary from one neighborhood to another, depending on contextual factors such as urban morphology and microclimate. In the case of Boston, densely-built urban neighborhoods in downtown area exhibit net life-cycle burdens of nearly 120 kg CO_2-eq/m^2 due to a 0.2 increase in road albedo, while net GWP savings can be observed in most low-density residential neighborhoods. This work provides insights into pavement albedo impacts at an urban scale and will help urban planners or decision makers to make informed decisions on whether pavement albedo enhancement is an option worth pursuing in a given urban area/neighborhood. Site-specific evaluation of pavement albedo impacts should ultimately be integrated into pavement LCA and guide decisions towards more sustainable pavement designs.

Thesis Supervisor: Franz-Josef Ulm
Title: Professor of Civil and Environmental Engineering

ACKNOWLEDGEMENTS

My experience at MIT has been amazing, full of challenges and life-changing to me. The journey started on August 23, 2011, when I became one of the MEng students in the CEE family. I have been given unique opportunities and taken advantage of them. With the guidance of Dr. E. Eric Adams, who is also one of my doctoral thesis committee members, I got to know life cycle assessment (LCA) and became fascinated about it. After the first year of study, I decided to extend my interest in LCA and pursue more challenging research at MIT. I was so lucky that I was given this opportunity to join MIT Concrete Sustainability Hub in 2013, where I have encountered dozens of remarkable individuals who I wish to acknowledge.

First of all, I would like to gratefully acknowledge the guidance, support and encouragement of my advisors Dr. Jeremy Gregory and Dr. Randolph Kirchain. Their continuous mentorship and expert advice have been invaluable throughout all stages of my doctoral study and research.

My sincere gratitude is reserved for Professor Franz-Josef Ulm, Professor Colette L. Heald and Dr. E. Eric Adams, for their invaluable insights and suggestions. I really appreciate their time, expertise and their challenges during every committee meetings, which motivated me think deeper about my research from various perspectives.

Very special thanks to Professor Leslie Norford from MIT Department of Architecture, for his expertise in building technology and his support with the tool his group has developed. Also thanks to Dr. Adam Schlosser and Dr. Liyi Xu, for their knowledge in the field of climate science and providing data throughout our collaboration.

I would like to thank our industry partners and the sponsors of this project, for giving me the opportunity to carry out my doctoral research and for their financial support. I learned a lot of useful insights from an industrial perspective during our TAG meetings every year.

A heartfelt thanks to the supportive lab MSL and active graduate community here at MIT, who have made my life outside research colorful. Special thanks to Terra, Donna, Kiley and Sarah for their hard work and taking care of logistics.

Words cannot express the feelings I have for my family and friends. I would like to thank them for their love and standing by my side whenever I needed. I could not have achieved this without their spiritual supports.

TABLE OF CONTENTS

List of Figures

Figure 4.10 Breakdown of use phase GWP impacts with uncertainties for conventional PCC and AC designs and reflective PCC and AC designs for Boston. Albedo impacts relative to baseline of average earth albedo (0.3)

List of Tables

CHAPTER 1 INTRODUCTION

1.1 Background

Life cycle assessment (LCA) is a systematic method to evaluate the environmental burdens of a product or process. It is an approach that examines a product "from cradle to grave" (or another specified boundary), accounting for all the inputs and outputs from every aspect of its life cycle. LCA has been applied to pavements as a way to support environmentally conscious pavement design decisions. For pavements, each phase of the life cycle – material production, construction, use, maintenance and rehabilitation (M&R), and end-of-life (EOL) – has impacts on the environment. While there have been numerous pavement LCAs, many studies choose a cradle-to-gate system boundary, focusing primarily on the material production and construction phase. However, since pavement typically remains in service for decades and supports millions of vehicles over its life, the use phase has the potential to be a dominant contributor to the overall environmental impact of pavements and therefore deserves attention.

The concept of applying LCA to pavements as an environmental assessment tool has been discussed and explored for many years. Over the past two decades, pavement LCA has been expanding throughout the world, but its implementation and adoption as a decision tool by state departments of transportation (DOTs) or other transportation agencies is still rare. The bulk of the existing pavement LCA literature contains studies and tools with different scopes and methodological approaches, which has hampered the widespread utilization of LCA by pavement engineers and policy makers *(1)*. One of the most important advances in this field is the incorporation of use phase impacts and the development of mechanistic models to assess the impacts of use phase components such as pavement vehicle interaction (PVI) *(2)* and pavement surface reflectivity, also known as "albedo" *(3)*.

Albedo accounts for the effect of solar reflectance of a pavement on the global warming potential. Two major effects associated with albedo are radiative forcing (RF) and urban heat island (UHI). Radiative forcing accounts for the direct reflectance of the incoming solar radiation, while UHI effect indirectly contributes to global warming by increasing the ambient temperature and the energy demand for cooling devices. According to a study in Los Angeles, pavements comprise one-eighth of the urban surface area (roofs account for another one-eighth of the area) (4). Because they represent a relatively large fraction of the total surface area, pavements are the primary targets for albedo increases, making this a noteworthy element of the pavement life cycle. The carbon dioxide-equivalent offset attributed to the reflectivity of the pavements can be estimated based on the work of Akbari et al. (5), as has been done in many pavement LCA studies (6). Akbari's model uses an offset rate of 2.55 kg CO_2-e/m^2 due to increased radiative forcing (RF) over the entire life of a pavement, and an offset of 4.85 g CO_2-e/m^2 per year due to decreased electricity consumption for every 0.01 increase of albedo (7). It is important to note that while the physical mechanism that underlies albedo is well documented, there is still uncertainty about their extent in real-world pavement installations. To reflect this, significant uncertainty is assigned to the magnitude of each of these effects.

Roofs and pavements, which constitute about 20-25% and 29-44% respectively of typical US urban surfaces (8), generally have lower albedos than their surrounding areas, making them a big target for combating climate change and UHI. Increasing worldwide surface albedo, starting in urban areas, can help fight climate change by offsetting radiative forcing from carbon dioxide (CO_2) and other climate forcing gases and aerosols. Installation of high-albedo "cool roofs" across urban areas could also reduce GHG emissions from fossil fuel derived electricity used for air conditioning. Several U.S. states have policies supporting cool roof installation to reduce energy usage, improve air quality, and alleviate the urban heat island effect. Cool pavements, however, have not been widely adopted as a standard practice, but can potentially contribute to the GHG reduction because of the larger percentage of urban surfaces covered by pavements.

While many studies have examined the direct and indirect impacts of urban surface albedo, looking broadly at large-scale albedo change due to urbanization or specifically at roof albedo modifications (e.g. cool roofs), the impacts of pavement albedo have not yet been extensively studied separately from roof albedo. Pavement albedo is much more complicated than roof albedo in that its impacts involve more interactions with adjacent buildings, urban geometry, vegetation, etc. Research gaps exist in quantifying the impacts of pavement albedo in terms of radiative forcing and buildings energy demand. Therefore, the proposed research will contribute to understanding the science underlying the two mechanisms of pavement albedo impacts, in particular how contextual factors may influence the quantification of the impacts. Scientific models and engineering tools adapted from existing models will be used to evaluate the context-specific global warming potential (GWP) of pavement albedo, which will then be integrated into the life cycle assessment (LCA) of pavements and guide decisions towards more sustainable pavement designs.

1.2 Literature Review and Gap Analysis

The existing body of literature has demonstrated two mechanisms associated with the impacts of changing surface albedo, as mentioned above, one directly through the change in the earth's radiative balance and the other related to the buildings energy demand as a result of incident radiation and ambient temperature change. Mostly, the radiative forcing mechanism was studied in the context of large-scale land use change such as deforestation and urbanization, and the building energy mechanism was usually investigated for a specific roof albedo enhancement. This section reviews some of the current studies on the two mechanisms respectively, and attempts to identify the research gaps in the literature.

15

Radiative Forcing

The term "radiative forcing" (RF) is defined as the change in net (down minus up) irradiance (solar plus long-wave; in W/m^2) at the tropopause or at the top of the atmosphere (TOA) due to an imposed change *(9)*. It describes any perturbation or imbalance in the radiative energy budget of the Earth-atmosphere system, which has the potential to lead to climate changes and thus results in a new equilibrium state of the climate system. A variety of forcing agents can cause such a perturbation including greenhouse gases, tropospheric aerosols, ozone, land-use change (surface albedo change), solar irradiance and aerosols from volcanic eruptions. RF is then used to estimate and compare the relative strength of different anthropogenic and natural forcing agents on climate change. Positive RFs represent global warming and negatives lead to global cooling. According to IPCC Assessment Report 5 (IPCC AR5) *(10)*, land cover change since pre-industrial times, primarily due to deforestation, have induced an overall increased surface albedo and a negative RF of -0.15 ± 0.10 W/m^2. The uncertainty range associated with this estimate is large and the level of scientific understanding is medium-low as reported by IPCC AR5. This albedo enhancement is providing a small offset, compared to the 1.6 W/m^2 forcing from carbon dioxide (CO_2) and the comparable forcing from non-CO_2 warming agents.

Studies have demonstrated that enhancing urban albedo can produce additional negative radiative forcing without the downside of environmental damage. It becomes useful to quantify the albedo-induced RF since it can to some extent mitigate or delay some of the consequences of warming from CO_2 emissions. Researchers at the Heat Island Group at the Lawrence Berkeley National Laboratory (LBNL) have attempted to quantify the relationship between surface albedo and radiative forcing. Akbari et al. estimate an average RF of -1.27 W/m^2 for an albedo increase of 0.01 based on global energy balance, and for every square meter of urban area, 2.55 kg of emitted CO_2 is offset for 0.01 increase in albedo due to increased radiative forcing *(5)*. The same paper also cites an alternative method that yields a higher offset of 4.90 kg of emitted CO_2 per m^2. These estimates of CO_2-e emissions offset from radiative forcing offer only a one-

time benefit and are based on annual average global insolation and cloud cover. Besides the analytical method, Menon et al. use a detailed land surface model developed by NASA to perform simulations of boreal summers (June to August) over a twelve-year period. Based on simulation-generated data, they calculated that the RF for a 0.01 albedo increase is -1.63 W/m^2 (11). Both studies indicate a reduction in radiative forcing or an increase in total outgoing radiation for an increase in urban albedo.

However, there is great uncertainty and spatial variability associated with these estimates due to the characterization of land cover, exclusion of feedbacks, and the climate model used to simulate the RFs. Locational and seasonal changes in albedo, cloud cover and insolation are not taken into account in most of the analytical studies. In addition, most of the existing works focus on the estimations of RF due to large-scale land cover changes such as deforestation, urbanization and greenhouse agriculture. Only a few studies have quantified the direct radiative impact as a result of the modifications to pavement surfaces. These research gaps need to be filled in order to better quantify the location-specific impact of pavement albedo in terms of RF and GWP.

Buildings Energy Demand

Changes in surface albedo due to urbanization have led to higher air temperature in the urban areas than their rural surroundings, known as the "urban heat island effect". Increased temperature in the summertime results in an increase in cooling demand for buildings and excess GHG emissions from producing the energy required to fulfill the needs. Akbari et al. reported that for the major metropolitan areas in the U.S., peak electricity load would increase by 1.5–2% for every 1°F increase in ambient temperature (12).

There has been growing interest in mitigating the UHI effect by using reflective materials for roofs and pavements. Reflective roofs can reduce cooling loads of buildings in summer, but increase heating loads in winter. The latter is known as the

"heating penalty" of high albedo. The relative magnitudes of cooling saving and heating penalties depend on a combination of multiple factors, including location, climate conditions, building types, the source of energy used for heating and cooling, etc. Akbari et al. found the largest net savings in the hottest and sunniest cities and that the savings decreased as the climate got cooler (13). Net savings were positive even in colder climates for most building types. Levinson and Akbari (2009) predicted that reflective roofs almost always reduced the annual cooling load more than it increased the annual heating load per-conditioned roof area, with the greatest savings in Hawaii and the least in Alaska (14). However, in a case study, Akbari and Konopacki (2005) conversely found that the use of reflective roofs would lead to larger heating penalties than cooling savings in electric heating residential buildings under cold climate conditions (15).

The impact of reflective pavements on buildings energy demand is more complicated as it is affected by the interaction between pavements and buildings, as well as the energy exchanges in surface-atmosphere interactions. Yaghoobian et al. (2010) found a cooling load saving of 17% in buildings due to a reduction in shortwave radiation transfer from the ground to nearby buildings by using low-albedo ground surfaces, rather than reflective pavements (16). In a later study, they found that increasing pavement albedo from 0.1 to 0.5 near a four-story office building in Phoenix would increase annual cooling loads up to 11% (33.1 kWh/m^2), while annual heating load was not sensitive to such a modification (17). These results indicate the potential of increasing cooling loads in adjacent buildings by absorbing more radiation from reflective pavements. Haley et al (2017) from LBNL assessed the energy and environmental consequences of cool pavements in Los Angeles and Fresno, California. Their work also reinforces the fact that the net effect of increased incident radiation and reduced ambient temperature on building energy due to pavement albedo increase is not intuitive.

There are research gaps existing in quantifying the buildings energy demand due to urban albedo modifications. Most of current studies focus on the reflective roofs rather than pavements. The effects of shadings on pavements and multiple reflections by

adjacent buildings on buildings energy demand have not been well understood. In addition, there is currently no analytical model for estimating the urban-scale buildings energy demand. The relationships between buildings energy demand and various contextual parameters such as urban configuration, building geometry, surface properties and climate condition still remain unknown.

1.3 Research Objectives

This study attempts to address the gaps in the literature by improving the understanding of the physics behind pavement albedo and the quantification of its impact on radiative balance and urban energy demand. The objective of the research is to evaluate how different mechanisms impact the overall life cycle environmental impacts of pavements under different circumstances by developing context-specific models for quantifying the impacts of pavement albedo on radiative forcing and buildings energy demand, taking into account various contextual parameters, and see To achieve the goal, simulations and parametric analyses are performed to investigate the relationships between various contextual factors and pavement albedo.

The analytical models will be incorporated into pavement life cycle assessment for a series of pavement albedo enhancement scenarios in selected locations and used to estimate the magnitudes of RF and BED induced by the pavement albedo enhancement, and compare with other climate change mitigation strategies to inform more sustainable pavement design decisions.

1.4 Research Questions

To achieve the above goals, several research questions concerning the two mechanisms of pavement albedo impacts have been framed as follows:

Radiative forcing

19

- Depending on the available data, what are the relationships between contextual characteristics such as solar insolation, cloudiness, etc., and the RF due to pavement albedo change?
- What are the uncertainties/accuracy associated with the relationships between pavement albedo and other contextual factors?

Building energy demand
- What are the mechanisms that drive changes in buildings energy demand due to the pavement albedo enhancement?
- What are the contextual factors that mostly strongly affect buildings energy demand due to albedo changes?

Pavement life cycle assessment
- How do these two mechanisms compare with each other? What's the net impact of pavement albedo under different contexts?

- How do albedo impacts compare with other components in a pavement's life cycle?

1.4 Research Methodology

To answer these research questions and achieve the goal, two types of models – analytical and numerical – have been proposed to quantify the impacts of changing pavement albedo. Model developments follow the four steps for both radiative forcing and buildings energy demand:
- Identify through literature review and preliminary analysis the contextual parameters that should be considered in the model
- Run numerical models to generate datasets for the analytical models or statistical models; investigate the locational and temporal patterns in the data and the potential relationships among parameters

- Building off the definitions and existing studies, develop the analytical models using the datasets from numerical models, taking into account the contextual factors and the uncertainties associated with them
- Validate the analytical models against existing studies, measured data or more complicated numerical models

1.5 Intellectual Contribution of the Dissertation

This dissertation fills in the gaps in the literature of pavement LCA and albedo impact quantification. It has the following contributions:

- Context-specific models for RF and BED are developed for quantifying the GWP impact of increasing pavement albedo.

- The physical and statistical relationships between pavement albedo and contextual characteristics have been investigated.

- The albedo models have been integrated into our probabilistic pavement LCA model for comparing the albedo impacts under the context of a pavement's life cycle.

- A four-step methodology has been proposed for applying the context-specific albedo models to any location with GIS data. The approach has been demonstrated through case studies on realistic neighborhoods in Boston and Phoenix.

- Case studies applying the models demonstrate that increasing pavement albedo has significant potential to mitigate impacts of climate change and UHI effects.

- Nationwide analysis show significant opportunity for RF benefits at the national level

- At urban scale, RF is more significant than BED in most neighborhoods and reflective pavements favor less dense neighborhoods
- Albedo can be a significant portion of pavement life cycle environmental impacts, but is context sensitive

1.6 Outline of the Dissertation

This dissertation has five main chapters. This first chapter starts with the background and existing gaps in the literature, bringing up the research questions, followed by the methodology proposed and the contributions to the field.

Chapter 2 describes an analytical model developed in this study as the main tool to assess radiative forcing (RF) impact of changing pavement albedo. Adapted from existing empirical model, the analytical model developed in this study takes into account a number of location-specific parameters including solar intensity, solar zenith angle, water content and cloudiness. The relationships among these parameters are investigated and modelled based on observational data from climate simulations.

Chapter 3 presents a modeling framework for estimating building energy demand (BED) due to changes in pavement albedo at an urban scale. While most of current building energy modeling programs focus on a single building envelope, they are hard to be scaled up to the urban scale. Energy performance of urban buildings is significantly impacted by interactions of components that constitute an urban built environment, including but not limited to local climate, building envelopes, ground surfaces, urban morphology, etc. To account for the interaction effects in an urban context, the modeling framework integrates three different engines: the core energy simulation engine – EnergyPlus™, the radiation shading engine – Ladybug & Honeybee, and the microclimate engine – Urban Weather Generator (UWG). A design of experiment (DOE) is conducted to investigate the relationship between urban morphology and BED due to pavement albedo change. Meta-models are developed based on the data obtained from the DOE, which are then used for estimating the albedo-

induced BED for any given neighborhood with only four input morphological input parameters extracted from realistic GIS databases.

In Chapter 4, the models presented in Chapter 2 and Chapter 3 are incorporated into the pavement LCA model, and used to evaluate the life cycle impact of different reflective pavement strategies.

The concluding chapter summarizes the findings on the relationship between pavement albedo and its impacts on RF and BED, and how they are affected by contextual factors. Limitations of the models are discussed and future work are proposed at the end.

CHAPTER 2   ANALYTICAL MODEL FOR QUANTIFYING RADIATIVE FORCING IMPACT OF PAVEMENT ALBEDO

2.1 Introduction

Urbanization (conversion of natural surfaces to man-made impervious land), as a result of population growth and economic development, has been noted as one of the principal human activities influencing the global climate. In the U.S., it is estimated that roof area fractions vary from 20% to 25% and pavement constitutes 29% to 44% of the urban areas *(8)*. These man-made surfaces usually absorb more incoming solar radiation, raise the ambient temperature, increase buildings' energy loads, and potentially exacerbate outdoor air quality and comfort issues. Among many technological strategies, increasing the albedo of the urban areas by increasing the reflectivity of the artificial urban surfaces (mainly roofs and pavements) has been proposed as an approach to mitigate the impacts of urban heat islands (UHI) and climate change resulting from anthropogenic activities.

Albedo, or solar reflectivity, is the ratio of solar radiation reflected by a surface to the amount incident upon it, ranging from 0 (complete absorption) to 1 (complete reflection). There are two known climate effects of changing surface albedos. One direct impact is through radiative forcing (RF), which measures the imbalance of the earth's energy budget at the top-of-atmosphere (TOA). Elevated surface albedo means that more solar radiation will be reflected back into space and less will remain on the earth. The change in the net outgoing radiation at TOA is called RF. The other climate-related effect of modifying surface albedo is through changes in buildings' energy demand (BED) for nearby buildings. Increase in urban surface albedo can both increase reflected radiation on nearby buildings and reduce the ambient temperature around buildings. These changes alter heating and cooling energy demands and their associated emissions.

This is an indirect impact of changing surface albedo. This study focuses on quantifying the former, direct RF effect.

Many studies have applied simple models to quantify the impact of land cover changes on global climate (18–25). The challenge in estimating the RF impact associated with land cover changes, however, lies in the difficulty in quantifying the transmittance of radiation through atmosphere and the uncertainties with temporal and spatial variations. Most of the current literature estimates RF impact due to large-scale land cover changes such as forestation/deforestation or greenhouse agriculture (19,23,24). In these studies, the impact of land cover change on transmittance is modeled following some global average radiative response for all locations (18,25). To the authors' knowledge, there is no context-specific expression that is suitable for estimating the RF impact specifically associated with man-made surface albedo modifications. In fact, the RF due to pavement albedo enhancement for a specific location depends largely on the local radiation intensity and atmospheric condition, which are affected by a lot of contextual factors such as solar angle, water content, and aerosols in the atmosphere. In addition, numerical simulations have been used to monitor the radiative balance at the TOA, but uncertainties exist due to the model resolutions and the simulation setups.

To fill in the gaps in the literature, we present an approach to calculate RF and the associated GWP impact due to albedo enhancement using an analytical approach adapted from a model-based parameterization. The approach aims to differentiate the impact by location and should prove to be useful to compare the effectiveness of albedo modification strategies in terms of GWP, and in life cycle assessments (LCA) so that the strategies can be compared to other life cycle elements (such as materials and construction). We first review the existing literature on estimating RF and GWP induced by albedo changes (mostly associated with large-scale land cover changes). Two different approaches are proposed for calculating the location-specific atmospheric transmittance factor, a key parameter in the RF estimation. Based on existing databases and simulated data, an adapted analytical model is then developed to calculate the upper and lower bounds of the GWP impacts due to albedo changes for 14 cities in the U.S

26

representing different climate conditions. Finally, the new model is applied to a nationwide study to demonstrate the effect of context on GWP savings from pavement albedo enhancement. The assumptions, strengths and limitations of various approaches are discussed in detail.

2.2 Approaches to Quantify RF Impact Due to Albedo Changes in the Literature

2.2.1 Calculating RF at TOA due to albedo changes

As defined by Ramaswamy et al *(9)*, the term "radiative forcing" (RF) is the change in net (down minus up) irradiance at the tropopause (typically measured in watts per square meter). For shortwave forcing agents like surface albedo changes, the instantaneous RF at the TOA is linked to surface temperature change and can be used instead of the stratospheric-adjusted RF at the tropopause *(26)*. Therefore, RF at TOA due to albedo change can be calculated as the change of shortwave radiation at TOA:

$$RF_{TOA} = -R_{TOA}\Delta\alpha_p \tag{2.1}$$

where the R_{TOA} is downward solar radiation at the TOA and $\Delta\alpha_p$ is a variation in planetary albedo. Following a procedure widely reported in the literature *(19,20,25,27)*, changes in planetary albedo $\Delta\alpha_p$ can be linearly related to changes in surface albedo $\Delta\alpha_s$:

$$\Delta\alpha_p = f_a\Delta\alpha_s \tag{2.2}$$

where f_a is a two-way transmittance factor accounting for absorption and reflection of solar radiation throughout the atmosphere. Convolving Eq. (2.1) and (2.2) we get

$$RF_{TOA} = -R_{TOA}\Delta\alpha_p = -R_{TOA}f_a\Delta\alpha_s \tag{2.3}$$

Lenton and Vaughan *(27)* further decompose f_a into downward and upward transmittance coefficients:

$$f_a = \frac{R_s}{R_{TOA}} \times \frac{R_{TOA,up}}{R_{S,up}} = K_T \times T_a \tag{2.4}$$

where R_s is downward solar radiation at the Earth's surface, $\frac{R_s}{R_{TOA}}$ is a downward transmittance coefficient - the fraction of R_{TOA} that reaches the Earth's surface (sometimes referred to as K_T), and T_a is an atmospheric transmittance factor expressing the fraction of the radiation reflected from the surface that reaches the TOA. Figure 2.1 illustrates the radiation mechanisms for K_T and T_a and how they link to each other through surface albedo α_s and planetary albedo α_p. R_{s_up} and R_{TOA_up} represent the reflected short radiations (upwelling) at the surface and TOA, respectively.
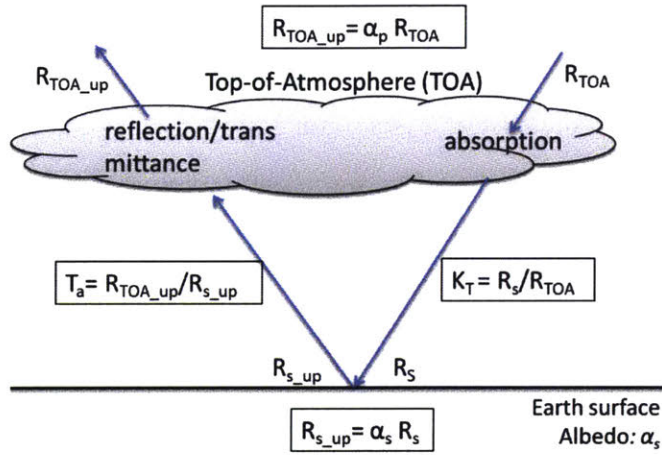
Figure 2.1 A schematic diagram showing downward and upward transmittance of solar radiation

From Eq. (2.3) and (2.4), RF at the TOA can also be computed using the solar radiation at the earth's surface:

$$RF_{TOA} = -R_s T_a \Delta \alpha_s \tag{2.5}$$

From these equations, we see that the albedo induced RF is a function of three quantities: the intensity of incoming radiation (R_{TOA} or R_s), atmospheric transmittance (f_a or T_a) and the change in albedo, $\Delta\alpha_s$. Of these, transmittance is particularly challenging to estimate. Generally, $\Delta\alpha_s$ would be known for a given situation off interest. Both R_{TOA} and R_s can be retrieved from various atmospheric databases (in the US a prominent one is made available online by NASA) or numerical simulation models such as the Weather

Research and Forecasting (WRF) model *(28)*. The transmittance factor f_a or T_a is not readily available and thus requires further investigation. The following section will summarize different approaches in the literature for evaluating the site-specific f_a or T_a based on otherwise available information.

2.2.2 Estimating transmittance factor f_a

Some early studies started using radiative transfer models to estimate f_a and T_a. From the clear-sky results of a *radiative transfer model*, Lacis and Hansen estimated an annual global mean value of f_a, which is 0.730 ($T_a = 0.854$) *(29)*. In a similar study later, Chen and Ohring estimated that f_a is 0.729 for a fixed solar zenith angle of 60°, and two different sets of empirical data yielded $f_a = 0.756$ and $f_a = 0.676$, respectively *(30)*. A different radiative transfer model that additionally includes aerosols and the variations in the albedo of different surfaces and solar zenith angle gives comparable clear-sky results *(31)*, i.e., for a solar zenith angle of 60° the maximum value of f_a is 0.759. Under cloudy skies, using a global average value of T_a (0.854), the global incident radiation at TOA and at the Earth's surface, Lenton and Vaughan *(27)* obtained a global average f_a value of 0.48. Overall, there are mainly two different analytical approaches for calculating f_a: a simple symmetric model and a model-based parameterization. Table briefly summarize the strengths, weaknesses and data required for each of the two methods.

Method 1: a simple symmetric model

As shown in Figure 2.1, f_a is defined as the effective "two-way" transmittance of the atmosphere and is a function of both K_T and T_a (See equation (4)). K_T can be estimated from satellite measurements of solar insolation at the earth's surface and, as such, can be retrieved freely online for any given location and time period ranging from a single month to 22 years *(28)*. It can also be calculated from R_s and R_{TOA} data from climate simulations. Values for T_a are not usually reported in the literature for specific locations. However, if one assumes that the same physical mechanisms influencing K_T (i.e., cloud albedo, molecular and gaseous absorption and scattering, aerosol scattering, etc.) also

influence the amount of radiation arriving back at the TOA after reflection at the surface (i.e. assuming the downward and upward paths are symmetric) *(20)*, we can estimate $T_a \approx K_T$. This allows us to rewrite Eq. (2.4) as:

$$f_a = K_T^2 \text{ or } T_a^2 \tag{2.6}$$

This approach is useful because f_a or by extension T_a can be estimated using the data sources available for K_T. The limitation of this approach is that it assumes that the downward and upward transmittances are approximately equal, which is not necessarily the case.

Method 2: Parametric model

As indicated in Eq.(2.2), there is a linear relationship between the planetary albedo α_p (or $\Delta\alpha_p$) and the surface albedo α_s (or $\Delta\alpha_s$). The gradient of this linear relationship between $\Delta\alpha_s$ and $\Delta\alpha_p$ is defined as the transmittance factor f_a. Based on observational data on α_s and α_p, Li and Garand found f_a to be significantly dependent on solar zenith angle, total precipitable water in the air, and cloud cover *(31)*. As solar zenith angle increases, f_a decreases from a maximum of 0.776 at 0° to 0.509 at 85° due to the greater absorption along longer path lengths of sunlight through the atmosphere *(30)*. A parameterization model was developed by Li and Garand that quantifies the gradient f_a from water vapor (proxied by precipitable water) and solar zenith angle *(31)*:

$$f_a = (1.16711 + 0.05963pw^{0.5} + (0.07514 + 0.04105pw^{0.5})/cz)^{-1} \tag{2.7}$$

where pw is the total precipitable water (in cm) and cz is the cosine of the solar zenith angle. It is important to note that Eq. (2.7) was derived using only data for clear-sky days (when cloud cover is 0%). As a result, clear-sky values for f_a estimated using this approach is considered as the maximum potential net transmittance and there could be an over-estimate of f_a as clouds are present some of the time everywhere.

This approach does not assume a symmetric (up-down) transmittance. This approach is limiting, however, due to the fact that the parameterization in Eq. (2.7) was specifically developed for clear-sky condition; the effect of cloud cover is missing. This work

addresses this shortcoming by developing a complementary statistical model of cloud transmittance.

Table 2.1 Comparison between the simple symmetric model and the model-based parameterization for estimating f_a

	Simple symmetric model	Model-based parameterization
Data required	Solar insolation at surface and TOA R_s, R_{TOA}	Precipitable water pw and cosine of solar zenith angle cz
Strengths	Location-specific data available; Implicitly include cloudiness effect	Location-specific data available; asymmetric transmittance
Limitations	Assume symmetric paths for simplicity	Cloudiness effect not accounted for
Reference	Bright et al (20); Lenton and Vaughan (27)	Li and Garand (31)

2.2.3 Translating RF to GWP associated with pavement albedo changes

In order to quantify the impact of albedo modifications, and compare that impact with other life cycle impacts associated with the modifications (materials, construction, use phase, etc.), we evaluate the GWP of those modifications. GWP is chosen as the metric for comparison as it is commonly used in life cycle assessment. The Intergovernmental Panel on Climate Change (IPCC) defines GWP of a greenhouse gas species i as the ratio of the integral of the RF from i over some period TH to the integral of the RF from some reference gas, r, over that same period TH (26). Formally, this is written as:

$$GWP_i = \frac{\int_0^{TH} RF_i(t)dt}{\int_0^{TH} RF_r(t)dt} \tag{2.8}$$

where TH is the time horizon, and RF_i is the global mean RF of gas component i.

This concept is readily extensible to non-gas-based forcings by reinterpreting i as any intervention that leads to a forcing. Following this formal calculation for GWP, we quantify the GWP due to unit change in pavement albedo over some period of time as

the ratio of the integral of the RF due to the albedo change over the effective analysis period (AP') to the RF due to CO_2 emissions over the period TH.

$$GWP_{alb} = \frac{\int_0^{AP'} \frac{A}{A_{earth}} \cdot RF_{alb}(t)dt}{\int_0^{TH} RF_{CO_2}\, dt} \tag{2.9}$$

where A is the unit area of pavement that is subject to albedo modification and AP' is the smaller of the analysis period (AP) and TH. Effectively, the numerator is the equivalent RF that a small unit area A would have at a global scale. For this study, we assume $AP = TH$.

2.3 Calculating Location-Specific RF Impact Due to Changes in Pavement Albedo

As demonstrated in the Section 2.2, models for calculating GWP and RF have been well established for clear-sky conditions. The key of the methodology proposed in this study is to develop a relationship between cloud transmittance and other contextual meteorological variables, and combining that with the model for clear-sky f_a. Applying this adapted parameterization model and the simple symmetric model yields the upper and lower bounds of the all-sky f_a value, and consequently an estimate of the range for GWP savings following three steps described below.

Step 1: Estimate transmittance factor f_a under cloudy sky conditions

Since the presence of clouds reduces the transmittance of incoming solar radiation, cloud transmittance factors have been modelled as modifiers of the clear-sky modelled radiation *(32–34)*. In our analysis, cloud effect is treated as a multiplier $g(cloud)$ to clear-sky f_{a_clear}, such that:

$$f_{a\_cloud} = f_{a\_clear} \cdot g(cloud) \tag{2.10}$$

A value of $g(cloud) = 1$ corresponds to a clear sky with no clouds, while $g(cloud) = 0$ indicates that no radiation reaches the surface, which will never happen in reality. Our goal will be to infer *g(cloud)* empirically using a parametrized model, however, as

32

discussed earlier fa cannot be directly observed. To overcome this, we assume that cloudiness has approximately the same effect on downwards as on upwards transmittance. If this holds, the same multiplier can also be applied to account for the reduced transmittance caused by cloudiness for the one-way transmittance coefficient K_T, as shown in the expression below:

$$K_{T\_cloud} = K_{T\_clear} \cdot g(cloud) \tag{2.11}$$

More directly, this means that we can infer $g(cloud)$ based on observations available about K_T.

A number of studies have attempted to model cloud transmittance based on precipitable water[31], the amount of clouds and cloud types [35], cloud optical depth [36], solar zenith angle, and diurnal temperature range [37]. Many of them achieved reasonably good estimations of cloud albedo or cloud transmittance under different contexts when validated against empirical results, and provide insights into error sources if models do not agree with measurements.

In our analysis, we explore the correlations between cloud transmittance and precipitable water, cloud fraction, diurnal temperature range, and solar zenith angle. These parameters were selected because of their conceptual basis in the literature and their availability for most locations in the United States. We make use of nine years of data collected from WRF simulations.

To ensure that there is no error introduced from using different data sources, we first calibrate the model proposed by Li and Garand (see Eq.(2.7)) for the one-way transmittance factor K_{T_clear} using our data set. We then explore different models for $g(cloud)$ to identify the model that best explains the difference (ratio) between the predicted K_{T_clear} and the observed cloudy-day K_{T_cloud} .

Filtering the data for only clear-sky days (cloudiness index = 0), we observed a good correlation among clearness index K_T, precipitable water pw, and cosine of solar zenith

angle cz (R-squared of 0.9). Figure 2.2 shows the scatter plot of actual K_{T_clear} versus K_{T_clear} predicted by this model:

$$K_{T\_clear} = f(pw^{0.5}, cz) \tag{2.12}$$
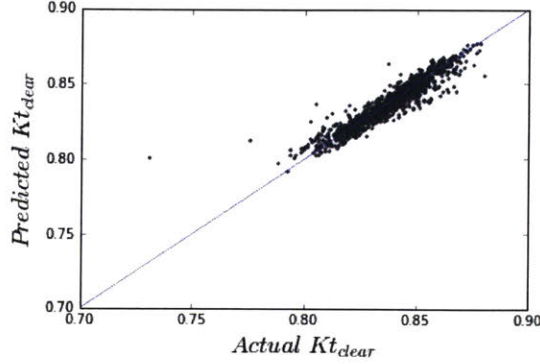
Figure 2.2 Scatter plot of predicted K_{T_clear} vs. actual K_{T_clear}. Also indicated is the 1:1 line

Next, we compute the cloud transmittance factor (cf), from the observed K_T for the all-sky condition as the ratio of K_T to the clear-sky K_{T_clear} predicted by the above model:

$$cf = K_T / K_{T\_clear} \tag{2.13}$$

where K_T is obtained from WRF simulations calculated as the ratio of downward solar radiation at the surface to that at the TOA, as in Eq. (2.4). Figure 2.3 shows the calculated daily cloud transmittance factor cf together with cloud fraction cld, the diurnal temperature range ΔT and the cosine of solar zenith angle cz. As expected, the cloud transmittance factor cf is clearly correlated with cloud fraction cld, with a correlation coefficient of -0.74. For example, a low cloud transmittance factor on 27 Jan, indicated by the dashed line in Figure 2.3, corresponds to an overcast condition with high cloud fraction, whereas the correspondence is less clear for ΔT and cz (correlation coefficient are 0.49 and 0.34, respectively).
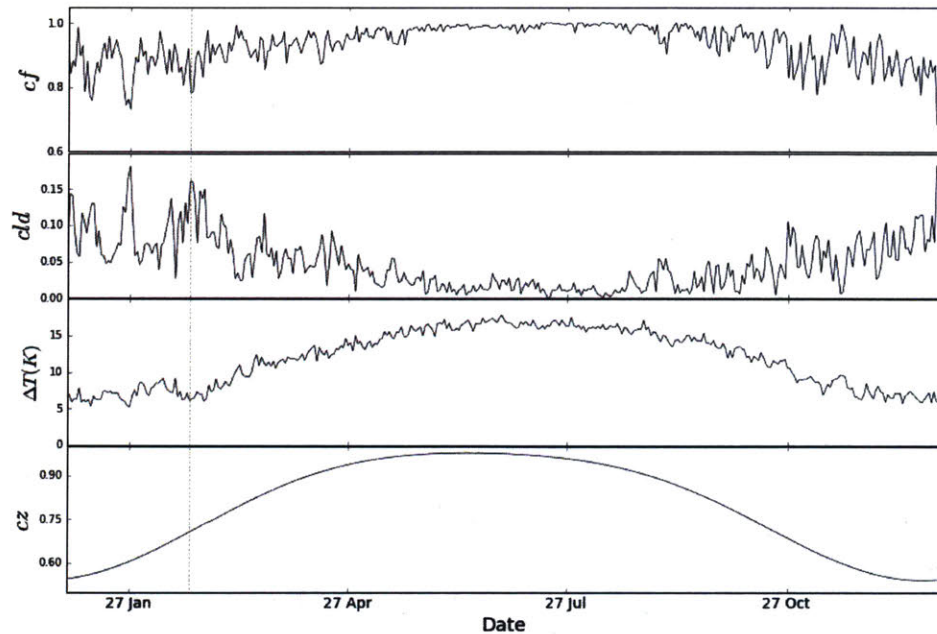
Figure 2.3 Daily cloud transmittance factors *cf*, together with daily cloud fraction *cld*, diurnal temperature range ΔT, and cosine of solar zenith angle *cz*. Dashed line denotes data for the 27th of January

We examine a range of linear and non-linear regression models to search for the best model that can be used to predict the cloud transmittance factor *cf*, using the three variables mentioned above. R-squared is used as an indication of the goodness of fit. Table 2.2 lists the parameterization results for all the models tested. Generally, different models perform similarly with R-squared values between 0.55 (linear function with only one independent variable *cloud*) and 0.57 (linear function with interaction term). It should be noted that cloud fraction itself explains 55.3% of the total variance. Adding cosine of solar zenith angle *cz* and diurnal temperature range ΔT, as well as their interaction term does not improve the linear model markedly. Polynomial, exponential, and Gaussian models yield similar R-squared values but they are more complicated in form.

35

Table 2.2 Regression models used in the regression analysis between the independent variables cloud fraction cld, cosine of solar zenith angle cz, and diurnal temperature range ΔT as independent variables and the dependent variable daily cloud transmittance factor cf. Also shown are the values of the coefficients and corresponding R-squared values for the regression equations that best fit to data pooled from WRF simulations.

Models	$cf = g(cloud) = f(cld, cz, \Delta T)$	Coefficients	R-squared
Linear 1	$cf = a \cdot cloud + b$	-1.25, 1.00	0.5530
Linear 2	$cf = a \cdot cloud + b \cdot cz + c$	-1.19, 0.097, 0.915	0.5656
Linear 3	$cf = a \cdot cloud + b \cdot cz + c \cdot \Delta T + d$	-1.17, 0.083, 0.001, 0.917	0.5657
Polynomial	$cf = a \cdot cloud^2 + b \cdot cloud + c$	1.38, -1.63, 1.00	0.5631
Linear w/ interaction term	$cf = a \cdot cloud + b \cdot cz + c \cdot cloud \cdot cz + d$	-1.86, 0.06, 0.97, 0.95	0.5716
Exponential	$cf = 1 - exp(- a \cdot cloud)$	462.06	0.5469
Gaussian	$cf = a \cdot exp[-(\frac{cloud-b}{c})^2]$	2.2E05, -16.14, 4.6	0.5670

Since no simple model can explain all the variability displayed by the cloud transmittance factors, we investigate the residuals of these regression models. Figure 2.4(a) shows the residual plot for the linear regression with interaction term, where the residuals are calculated as the difference between the fitted cf and measured cf. It is obvious that parameterized cloud transmittance factors deviate from the measured cloud transmittance factors and the deviation is greater for low cloud transmittance factors (corresponding to cloudy-sky conditions). The heteroscedasticity implies that the default assumption for least squares regression – that is, the random errors have a constant standard deviation – may not hold. Weighted least squares (WLS) regression is then applied to address this problem. This method tries to give each data point its proper amount of influence over the parameter estimates. Different types of weighting are applied including absolute values, log of squared residuals, squared residuals and squared fitted values. The one that performs the best is making the adjustment proportional to the squared fitted values of cloud fraction $cloud$. The resulting weighted residual plot is shown in Figure 2.4(b), which clearly demonstrates the improvement by

reducing the heteroscedasticity. The WLS regression model has the following coefficients with an R-squared of 0.6163.

$$cf = g(cloud) = -1.54 \cdot cloud + 0.09 \cdot cz + 0.65 \cdot cloud \cdot cz + 0.92 \qquad (2.14)$$
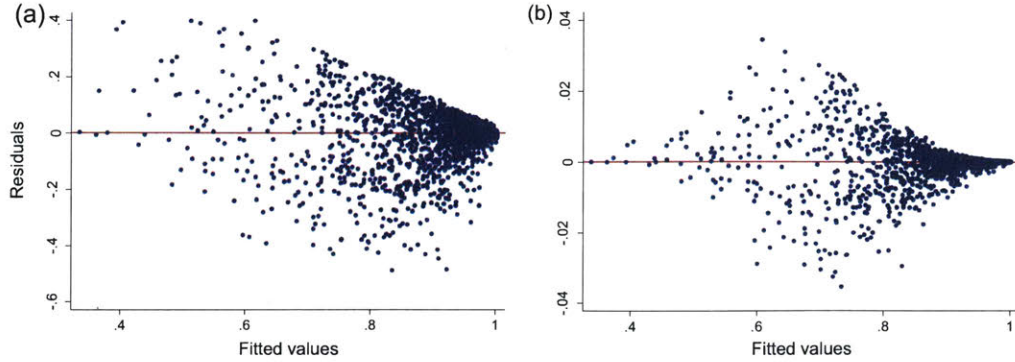
Figure 2.4 Residual plots for (a) linear regression model with interaction term and (b) weighted least squares (WLS) regression model

Combining the model-based parameterization and cloudiness regression model, we have an adapted model for cloudy-sky:

$$f_{a\_cloud} = f_{a\_clear} \cdot g(cloud) \qquad (2.15)$$

where f_{a_clear} is calculated using Eq.(2.12) and $g(cloud)$ is calculated using the weighted least square regression model in Eq.(2.14) with cloud fraction and solar zenith angle as the input variables. This adapted model yields an upper bound of f_a value.

Step 2: Calculate ranges of GWP

To compare the GWP impacts specifically related to changes in pavement albedo, we follow the approach described in Step 1 to calculate the lower and upper bounds of f_a values for a given location, and then apply the f_a values to Eq.(2.3) and (2.9) in Section 2, we have:

$$GWP_{alb} = \frac{-\int_0^{AP\prime} \frac{A}{A_{earth}} \cdot R_{TOA} \cdot f_a \cdot \Delta\alpha_s \, dt}{\int_0^{TH} RF_{CO_2} \, dt} \qquad (2.16)$$

In this study, the functional unit is defined as a square meter (m^2) of pavement. A_{earth} is the area of the earth, which is 5.1×10^{14} m^2. The R_{TOA} data is provided for each day

between 2000 and 2008. We set AP=50 years to be similar with common temporal scopes used in pavement LCAs. We evaluate a 100-year GWP (TH = 100) *(26)*.

All RF values due to an albedo change are normalized to a 0.01 increase in albedo) ($\Delta\alpha_s$ = 0.01). Applying equations (2.6) and (2.15), location-specific lower and upper bounds of f_a were calculated at a daily basis. The annual average f_a was computed from these values to arrive at the range of GWP savings for the entire analysis period.

Step 3: Incorporate urban transmittance to account for the shading effect in urban areas

The range of GWP savings calculated from step 2 only applies to unshaded roads in an open area. When estimating the transmittance factor, it implicitly assumes that 100% of the downward solar radiation transmitted through the atmosphere will strike on the unit area of pavement and there is no loss at the pavement surface. However, in a realistic urban setting, pavements are usually surrounded by buildings or trees, which block the sunlight and limit the amount of solar radiation that reaches the pavements. Therefore, to account for the effect of shading in an urban canyon, we further introduce an urban canyon transmittance, τ, which is defined as the ratio of the solar radiation reflected from the pavement surface at the bottom of an urban canyon, to the radiation reflected from the same road surface not in a canyon. It can also be interpreted as the transmittance or reflectance of an urban canyon. The value of τ should approach one as canyon height approaches zero, and should never exceed one. We rewrite Eq.(2.2) to include the total transmittance of the atmosphere and transmittance of the urban canyon:

$$\Delta\alpha_p = \tau \cdot f_a \Delta\alpha_s \tag{2.17}$$

Substituting Eq.(2.1) with Eq.(2.17) and rewrite Eq. (2.16), we have

$$GWP_{alb} = \frac{-\int_0^{TH} \frac{A}{A_{earth}} \cdot R_{TOA} \cdot \tau \cdot f_a \cdot \Delta\alpha_s \, dt}{\int_0^{TH} RF_{CO_2} \, dt} \tag{2.18}$$

We estimate the value of the urban canyon transmittance τ as 0.4 using a radiative transfer model described in the Urban Weather Generator model *(38)*, where the reflected solar radiation from a shaded road surface in an urban canyon and that from

38

an unshaded road can be explicitly calculated. It should be noted that the urban canyon transmittance τ is only applicable to urban areas. For rural areas, FHWA Roadside Design Guide requires a clear zone or horizontal clearance, which specifies a minimum unobstructed distance beyond the edge of the traveled way *(39)*. Therefore, τ equals 1 since little or no shading effect is expected to present in those areas.

2.4 Case Study

The objective of this case study is to apply the step-by-step methodology proposed above and quantify the GWP savings of increasing pavement albedo under different contexts. Fourteen cities across the U.S. are selected in this case study, representing seven major climate zones defined by the International Energy Conservation Code (IECC), as shown in Figure 2.5. The number 1 through 7 reflects the relative temperature ranging from 1 being 'very hot' to 7 being 'very cold'. The type of climate associated with each combination is specified in the legend of the map on the left corner. Notice that the IECC map also shows sub climate zones determined by moisture. Generally, it's moist in the East, dry in the West, and marine along the West Coast, indicated with letters A, B and C, respectively. To incorporate as many climate zones as possible, we choose twelve distinct combinations of sub climate zones in total within the seven major climate zones: Miami (1), Phoenix (2), Atlanta (3A), LA (zone 3B), San Francisco (3C), Baltimore (zone 4A), Seattle (4C), Boston (5A), Denver (5B), and Minneapolis (6), and Duluth (7). In addition, to understand the variation within one climate zone, we purposely select an additional two cities, Nashville and St. Louis, within climate zone 4A, in addition to Baltimore.

Marine (C)   Dry (B)   Moist (A)

Climate zone 1 -- Very hot-humid – Miami FL
Climate zone 2A -- Hot-humid – Houston, TX
Climate zone 2B -- Hot-dry – Phoenix, AZ
Climate zone 3A – Warm-humid – Atlanta, GA
Climate zone 3B – Warm-dry – Los Angeles, CA
Climate zone 3C – Warm-marine – San Francisco, CA
Climate zone 4A -- Mixed-humid – Baltimore, MD
Climate zone 4C -- Mixed-marine – Seattle, WA

Climate zone 5A – Cool-humid – Boston, MA
Climate zone 5B – Cool-dry – Denver, CO
Climate zone 6 – Cold-humid – Minneapolis, MN
Climate zone 7 – Very cold – Duluth, MN

Figure 2.5 Climate zones in the U.S. defined by IECC and the 14 cities representative of different climate zones

The location and climate information of the fourteen cities chosen are summarized in Table 2.3. The latitude of the urban area usually determines the intensity of the incoming solar radiation, and the amount of solar radiation transmitted through the atmosphere is dependent on the climate condition. For easy comparison across results within this study as well as reported numbers in the literature, in this analysis, we calculated the ranges of GWP savings due to an increase in pavement albedo normalized to 0.01 ($\Delta\alpha_s = 0.01$) for one square meter of pavement area in the 14 chosen cities over an analysis period of 50 years.

Furthermore, we perform a nationwide analysis of the transmittance factor f_a following the steps in Section 3 and calculate the GWP savings at a state level by using results from the nearest city, in order to gain an understanding of how context affects the impact of pavement albedo enhancement across the country.

Table 2.3 Location and climate information for cities selected for the case study

City	Location coordinates (Latitude, Longitude)	Climate zone*
Miami, FL	(25.76°N, 80.19°W)	1 (very hot-humid)
Houston, TX	(29.76°N, 95.38°W)	2A (hot-humid)
Phoenix, AZ	(33.45°N, 112.07°W)	2B (hot-dry)
Atlanta, GA	(33.75°N, 84.39°W)	3A (warm-humid)
Los Angeles, CA	(34.05°N, 118.25°W)	3B (warm-dry)
San Francisco, CA	(37.77°N, 122.42°W)	3C (warm-marine)
Baltimore, MD	(39.29°N, 76.61°W)	4A (mixed-humid)
Nashville, TN	(36.16°N, 86.78°W)	4A (mixed-humid)
St. Louis, MO	(38.63°N, -90.20°W)	4A (mixed-humid)
Seattle, WA	(47.61°N, 122.33°W)	4C (mixed-marine)
Boston, MA	(42.36°N, 71.06°W)	5A (cool-humid)
Denver, CO	(39.74°N, 104.99°W)	5B (cool-dry)
Minneapolis, MN	(44.98°N, 93.26°W)	6 (cold-humid)
Duluth, MN	(46.79°N, 92.1°W)	7 (very cold)

*Climate zones classified based on Briggs et al. *(40)*

Data source

WRF (the Weather Research and Forecasting model) is used in this study to populate location-specific data on solar radiation and other atmospheric parameters required for calculating the RF impact of pavement albedo change. The modeling domain spans the continental U.S. with a spatial resolution of 50 km, and the simulation is run continuously for 9 years from 2000 to 2008. An alternative data source could be the NASA Surface Meteorology and Solar Energy (SSE) online database, which provides 22 years (July 1983 - June 2005) of satellite measured data on solar insolation R_s and R_{TOA} *(28)*. This global and contiguous dataset is a result of re-analysis based on satellite measurements and models, as surface measurements are sparse or nonexistent over some regions.

Since the WRF simulated data has a better resolution and is more internally consistent than the NASA dataset, we perform the 14-city analysis and the nationwide analysis using data extracted from the WRF simulation. Variables to extract include downward solar radiation at the surface R_s (SWDOWN in WRF), downward solar radiation at the TOA R_{TOA} (SWDNT in WRF), precipitable water (*pw in* WRF), cosine of solar zenith

angle *cz* (COSZEN in WRF) and cloud fraction *cld* (CLDFRA in WRF). For each variable, daily average values are computed from hourly data in WRF.

Results and discussions

Following the 3-step methodology, the ranges of GWP savings from a 0.01 increase in pavement albedo are calculated for the 14 chosen cities, as shown in Figure 2.6. The upper bounds and lower bounds represent results calculated using the two different models described above: the symmetric model and our parameterization model adapted from Li and Garand (1994) with cloud transmittance effect incorporated. Cloud transmittance factors f_a are also plotted with red triangles on the y-axis. The ranges in GWP savings reflect the uncertainty associated with the climate condition. It can be seen from the figure that the uncertainty is closely correlated with the cloudiness of the area, which affects the transmittance of the solar radiation. Uncertainty is smallest for Phoenix as it's mostly clear in Phoenix throughout a year. For Miami and LA, uncertainty might arise from humid air, aerosols, or smog. Seattle experiences many cloudy and humid days throughout a year, so the range of uncertainty in GWP savings is also significant.

Across the 14 cities, the difference in results also indicates that the magnitude of the albedo-induced RF and the associated GWP savings are dependent on the context. While all 14 locations benefit from an increase in albedo, Miami and Phoenix present a greater opportunity for global warming mitigation through installations of reflective surface materials. In fact, the impact of albedo change in those two locations is nearly 50% greater than that estimated for Duluth. The spatial variations suggest that to fully understand the climate effects of reflective pavements, more detailed context-specific data will be required at a granular level.

Since the effect of shadings is included in the calculation, the estimated GWP savings in this analysis (0.90 to 1.77 kg $CO_{2\text{-eq}}/m^2$) is generally lower than the numbers reported in the literature, which range from 1.6 to 8.3 kg $CO_{2\text{-eq}}/m^2$. This could be explained by

the fact that in many other studies the GWP impacts from RF are estimated for albedo changes in large-scale, usually unshaded land covers.
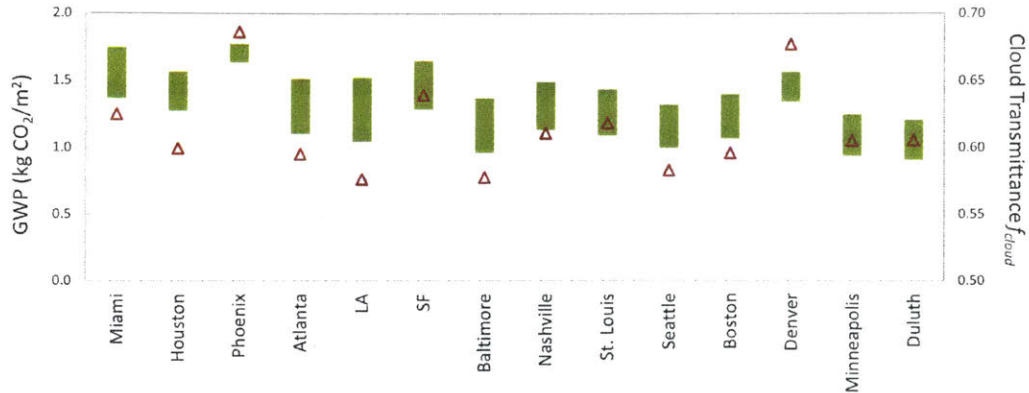
Figure 2.6 GWP savings from RF due to 0.01 increase in pavement albedo for the selected 14 locations over a 50-year analysis period using two models.

From the fourteen-city analysis results, we also notice that the three cities within the same sub climate zone 4a, Baltimore, Nashville and St. Louis, yield GWP savings very close to each other, with a difference smaller than 8%. This suggests our approach of choosing one city within one distinct climate zone and using the results of that city to represent the climate zone should provide a reasonable estimate of impact. In the following nationwide analysis, we apply a single value averaged across the three cities in the climate zone 4a to represent the GWP saving for that climate zone.

The detailed results with an interactive feature in Tableau workbook can be accessed via this link*. The nationwide analysis of cloud transmittance and GWP savings due to a 0.2 increase in pavement albedo is conducted at a state level and the results are shown in Figure 2.7 and in a Tableau dashboard. In this analysis, we assume that the albedo of all pavements across the U.S. is increased by 0.2. We then obtain data about total pavement area by state estimated by FHWA, and multiply them by the corresponding GWP savings per square meter of pavement for that state, calculated from our adapted model. The national map clearly demonstrates the variation in GWP savings across the country, depending on location and climate zone. In general, states in the south of U.S. have larger potential for CO_2 savings from RF due to pavement albedo enhancement,

* https://public.tableau.com/profile/xin.xu7844#!/vizhome/GWPsavings-Countylevel/Countylevel_unit

mainly because these states receive more solar radiation and have more roads exposed to sunlight. Texas exhibits the greatest GWP savings if all roads were converted into reflective pavement. The relative lower GWP savings in California compared to other states at a similar latitude is probably due to the climate condition particularly the cloudiness effect. This map shows the significance of context in impacting the RF and the effectiveness of GWP savings strategies. A granular analysis at a county level greatly improves the accuracy and reliability of the results.
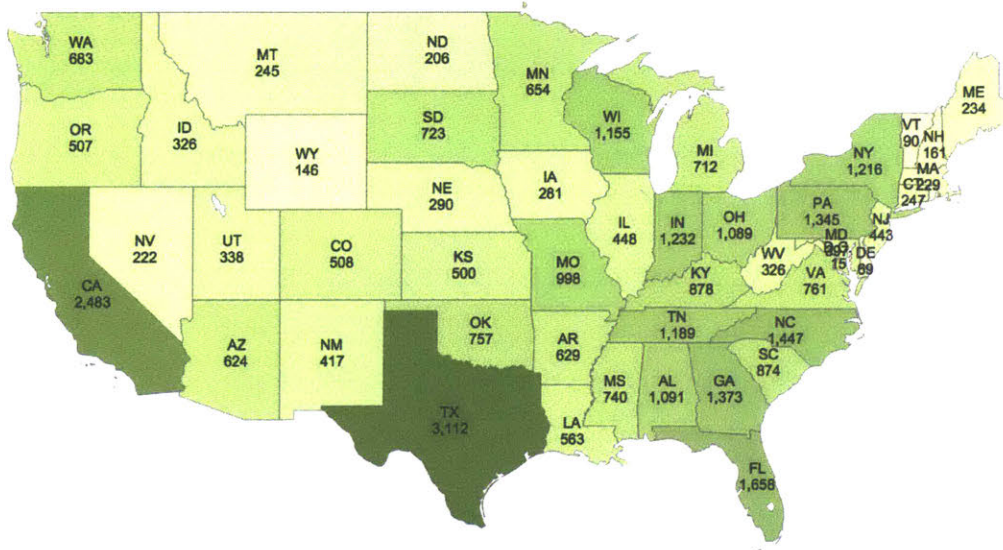
Figure 2.7 Annual GWP savings (kton CO_2-eq) from RF due to a 0.2 albedo increase for all urban and rural roads across the U.S.

2.5 Conclusions

Guidance on how to calculate the RF and corresponding GWP impacts due to pavement albedo changes is presented here. We adapt a model-based parameterization from the literature and additionally incorporate the effects of cloudiness and shadings in the urban area. Two research questions have been answered through model development and case studies:

- What are the relationships between contextual characteristics such as solar insolation, cloudiness, etc., and the RF due to pavement albedo change?

- What are the uncertainties/accuracy associated with the relationships between pavement albedo and other contextual factors?

In the adapted model we develop, the effects of solar intensity, precipitable water, solar zenith angle and cloudiness on atmospheric transmittance are parameterized and calibrated using data from climate simulation. Data and model indicate that the transmittance factor has a positive correlation with solar intensity, and negative correlations with precipitable water, solar angle and cloudiness. A case study of the RF impact due to pavement albedo modifications in fourteen major U.S. cities is conducted, with location-specific data extracted from sophisticated climate simulations. Ranges of the GWP savings reflect the uncertainties associated with the atmospheric transmittance, especially the cloudiness effect. Comparison of the results across the U.S. also reveals the spatial variation due to contextual variables.

In section 2.2, two different approaches are used to estimate f_a using the WRF data, following Eq.(2.6) and (2.15). For the case of Phoenix, the resulting mean f_a calculated from the simple symmetric model Eq. (2.6) is 0.617, and 0.729 from the parameterization model shown in Eq. (2.15). The discrepancy reveals different underlying assumptions regarding the downward and upward transmittance through the atmosphere. The symmetric model assumes symmetric processes and results in a smaller f_a (more is lost through the atmosphere than transmitted), while the parameterization is derived under clear-sky conditions so it will be an over-estimate as clouds are present some of the time everywhere. The adapted model we propose, however, partially addresses the limitation of the parameterized model by incorporating a cloudiness regression function $g(cloud)$. The f_a value calculated with this model is 0.683, which is greater than the f_a estimated from simple symmetric model, and smaller than the clear-sky f_a calculated using Eq. (2.7). The range computed from the symmetric model and the adapted model is a more accurate estimate of the f_a value and thus the associated GWP.

45

The adapted analytical model we propose offers an alternative computational approach to climate modeling, which can be easily applied to any geographic area. However, there are some limitations of the current model that could be improved in further research. First of all, the analytical model described above uses an average value of 0.4 for the effect of shadings. The urban transmittance factor τ can also be context-dependent, as it can be affected by the urban geometry such as building height and density, vegetation, etc. Further simulation is required to validate the urban canyon transmittance under different conditions. In addition, data on the evolution of pavement albedo is limited. The evolution of pavement albedo over time and its variability across a network should been incorporated into the model to account for the true of albedo as such data become available.

CHAPTER 3 MODELING THE IMPACT OF PAVEMENT ALBEDO ON URBAN ENERGY DEMAND

3.1 Introduction

Cities consume around three-quarters of global primary energy and account for 50% to 60% of the world's total greenhouse gas emissions *(41)*. The building sector is one of the most significant contributors to energy consumption and carbon emissions in urban areas, which means it has great potential for energy and carbon reductions *(42)*. The desire to meet carbon reduction and sustainable urban development targets has led urban planners and stakeholders to adopt various technological strategies, including cool roofs and cool pavements as effective ways to achieve the goal by reducing urban building energy demand (BED). We seek to quantify the impact of pavement albedo on BED in order to understand the contexts under which it can be considered a cool pavement strategy.

Impact of pavement albedo

Urban surfaces, including roofs and pavements, play an important role in shaping the urban microclimate, altering the energy balance and contributing to the so-called urban heat island (UHI) effect *(43)*. Albedo is a measure of the reflectivity of surfaces. It is defined as the ratio of solar radiation reflected by a surface to the amount incident upon it, ranging from 0 (complete absorption) to 1 (complete reflection). Increasing the albedo of road surfaces has a direct impact on adjacent buildings by incurring more *incident radiation* on the nearby buildings, resulting in changes in building energy consumption. It also reduces the *ambient temperature* within the canyon, altering BED in a way contradictory to the effects induced by increased *incident radiation*. Haley et al (2017) assessed the energy and environmental consequences of cool pavements for several cases in two locations in California. Their work reinforces the fact that the net effect of increased incident radiation and reduced ambient temperature on building energy due to pavement albedo increase is not intuitive. It requires a better

47

understanding of the relationship between urban morphology and building energy performance, as well as a modelling framework to predict BED in urban contexts.

Urban morphology

Urban morphology, or urban texture, is referred to as the spatial configuration of buildings in a city *(44)*. Studies have investigated the effect of urban morphology on the thermal behavior inside and outside the building, demonstrating the variation in energy performance induced by different urban textures *(45–50)*. Rode et al (2013) estimated theoretical heat-energy demand of different types of urban form at a scale of 500 by 500 meters, and found that urban morphology induced heat energy efficiency is significant and can lead to a difference in heat energy demand up to a factor of six *(45)*. Pisello et al (2014) observed a non-negligible difference (defined by them as Inter-Building Effect) when comparing building energy performance with and without realistic urban contexts *(51)*. Salvati et al (2015) characterized urban textures and confirmed the relevance of urban morphology to UHI intensity and BED *(52)*. These studies have shown that urban morphology has a significant impact on the urban microclimate and thus affects BED. However, no one has quantitatively estimated the impact of pavement albedo on BED and its variability in relation to urban morphology. As a result, the effectiveness of pavement albedo enhancement strategies for energy savings under different urban contexts is unknown.

Existing modeling frameworks

Most existing building energy models consider individual buildings as stand-alone entities, without any neighborhood contextualization *(53)*. These models simulate the energy balances on building envelope and indoor air, excluding the dynamic modeling of outdoor energy balance. They have been effective for evaluating different energy efficiency improvement strategies regarding modifications in building materials, structures and operations. By contrast, urban energy balance models in the meteorological community, such as urban canopy models (UCM), usually consider an urban grid cell as a 1-D or 2-D canopy consisting of a single building and canyon floor, which is an oversimplified representation of urban morphology *(54)*. In reality, the components of the outdoor environment (buildings, streets, vegetation, etc.) have

48

complex interactions with each other, which suggests a far more sophisticated system boundary and energy exchanges than that of individual building envelop or simple urban canopy. No single mathematical model exists that can address the complex physical phenomena in urban climate.

In recent years, research and modelling efforts have been devoted to investigating the interactions between buildings and the surrounding environment, accounting for the outdoor energy balance and the indoor-outdoor exchanges *(55–60)*. Most of the modelling frameworks require a co-simulation environment between building energy simulation engines and urban-scale simulation engines, which allow for urban parameterization at multiple scales. Kikegawa et al. (2003) coupled a one dimensional urban canopy meteorological model with a simple sub-model for building energy analysis *(55)*. Salamanca et al. (2010) developed a building energy model (BEM) with an urban canopy parameterization for mesoscale models *(57)*. Mauree et al (2017) recently coupled the Canopy Interface Model (CIM) with CitySim, an urban energy modeling tool, to simulate the energy performance of buildings with different urban forms and local climate *(60)*. While these coupled models have been successfully implemented and validated against measured data, they were limited to a few variations of urban form and context. Therefore, it's difficult to generalize the results to a larger scale. Quan et al (2014) studied the density-energy relationship through a parametric study to explore how density, building shapes and building typology jointly influence building energy performance, but they didn't account for the interaction between BED and urban microclimate *(61)*. None of the previous studies addressed the specific issue of how ground surface energy balance would affect BED, with one exception. Yaghoobian and Kleissl (2012), investigated the effect of albedo changes in the urban canopy floor surface on building thermal loads using the Temperature of Urban Facets Indoor–Outdoor Building Energy Simulator (TUF-IOBES), but they did not examine the impact of urban morphology *(17)*.

49

Contribution of this study

In order to evaluate the effectiveness of pavement albedo modification strategies and guide future urban planning or design decisions, more detailed quantitative study about the impact of urban morphology on local climate and the energy demand of buildings is necessary. This paper aims to investigate the direct and indirect impacts of changing pavement albedo on building energy performance, and their relevance to urban morphology and microclimate. An integrated modeling framework combining energy, radiation, and urban climate simulation engines is developed to simulate BED under different urban contexts. Taking a parametric approach, urban morphology is characterized and varied to examine the relationships between BED and various morphological parameters. Two major research questions are addressed:

- How does pavement albedo affect BED and what are the mechanisms?
- What is the change in annual heating/cooling energy demand due to pavement albedo changes for different neighborhoods with various morphologies?

In Section 3.2, we introduce the coupled modeling methodology and give a brief description of different models. The experimental design for the parametric analysis to examine the relationships among pavement albedo, urban morphology and BED is also presented in this section. Results from a case study on Boston and Phoenix using this methodology are shown in Section 3.3, followed by conclusions and discussion in Section 3.4.

3.2 Methodology

To address the limitations of existing building modeling frameworks mentioned above, the methodology proposed here is based on a bottom-up approach combined with a statistical method, allowing for more detailed neighborhood characterization while keeping it computationally efficient. There are four steps. In the first step, urban geometry is created using a geometric generation tool Rhinoceros® (Rhino) and Grasshopper® *(62)*. Second, parametric analysis is conducted to investigate the relationships between BED and urban morphology. Idealized neighborhood samples are

50

generated with different combinations of morphological parameters and the changes in BED due to incident radiation (ΔE_R) resulting from changes in pavement albedo ($\Delta \alpha$) are simulated for each neighborhood. In the meantime, each neighborhood is assigned a local climate zone (LCZ) based on an urban microclimate categorization scheme developed by Stewart & Oke (2012) *(63)*. Changes in ambient temperature (ΔT) due to the same change of pavement albedo are then simulated for each LCZ using an urban climate simulation engine - Urban Weather Generator (UWG) *(38)*, and the modified weather file is used to simulate the changes in BED due to ambient temperature change (ΔE_T). Third, because the generation of realistic neighborhoods is difficult and individual-building level energy simulation is time-consuming, a statistical meta-model is developed for each LCZ based on the inputs, i.e., morphology variables from the parametric analysis, and the output, i.e., changes in BED as a result of changes in incident radiation and ambient temperature ($\Delta E = \Delta E_R + \Delta E_T$). Finally, in order to demonstrate the methodology in a realistic urban setting, detailed information related to the morphology of real neighborhoods is extracted from GIS at the building level. Each building is assigned an LCZ where the building is located. The meta-models can then be applied to predict change in BED for every building within any realistic urban context, based on the extracted morphological parameters.

We use a hybrid modeling framework to implement the methodology, which combines the capabilities of several existing tools, including the geometric generation tool Rhinoceros®(Rhino) and Grasshopper® *(62)*, the energy and radiation simulation plugin for Grasshopper® - Ladybug and Honeybee *(64)*, and the urban climate simulator - Urban Weather Generator (UWG). The workflow is shown in Figure 3.1.

STEPS	TOOLS	OUTPUTS
Step 1 Urban geometry generation	Rhinoceros / grasshopper	
Step 2 Parametric design of experiments & building energy simulations	Urban Weather Generator (UWG)	ΔE_R & ΔE_T LCZ
Step 3 Meta-model development	Neural Networks input layer hidden layer 1 hidden layer 2 output layer	$\Delta\alpha$ ρ_b H/W S/V ⋮ ΔE Meta-models
Step 4 Application with GIS data	GIS Data	*Morphological parameters & ΔE*

Figure 3.1 Modeling framework for studying the impact of pavement albedo ($\Delta\alpha$ is pavement albedo change; ΔE_R is the change in BED due to incident radiation; ΔE_T is the change in BED due to ambient temperature)

3.2.1 Urban geometry generation: Rhino with Grasshopper®

The 3D urban geometries are generated within Rhinoceros® (Rhino), a CAD-based modeling environment used by urban designers and architects that allows for the integration of microclimatic considerations with the massing design *(65)*. Grasshopper® is a plugin for Rhino that allows for algorithmic modeling and parametric simulations. In order to perform the characterization of urban morphology that provides spatial context for buildings, this study defines a reference neighborhood as several close and contiguous building blocks with similar characteristics and the street network in between. The scale of the neighborhood is defined based on the LCZ. According to Stewart & Oke (2012), urban neighborhoods can be grouped into ten different LCZs based on their physical characteristics and surface properties (Table 3.1) *(63)*. The size of an LCZ typically spans from 400 meters to one kilometer, and buildings within an LCZ shares the same microclimate regime that influences building energy performance. For the purpose of this study, a dynamic building block matrix with 30 buildings is considered as the reference site for the parametric analysis. The area of the reference site should not be too small, so that it is not representative of the urban fabric, and also

not too large, comprising too many different structures. The building block matrix within the reference site consists of three building blocks, each with 2 × 5 buildings, separated by two pavements in between, as shown in Figure 3.2. The building in the center of the middle row (indicated with white roof) is the reference building of interest for energy or radiation simulations. In Rhino, the process of generating idealized samples of urban neighborhood is automated by changing the spatial parameters within the ranges specified for each LCZ in Table 3.1, which are observed ranges based on empirical studies. This also ensures that the idealized samples "look like" the real samples.

Table 3.1 Physical characteristics for the 10 local climate zones (*Source: Stewart & Oke, 2012) (63).*

Local climate zone (LCZ)	Canyon aspect ratio	Building density	Average building height (m)	Sky view factor
LCZ 1 Compact high-rise	>2	0.4-0.6	>25	0.2-0.4
LCZ 2 Compact mid-rise	0.75-1.5	0.4-0.7	8-20	0.3-0.6
LCZ 3 Compact low-rise	0.75-1.5	0.4-0.7	3-8	0.2-0.6
LCZ 4 Open high-rise	0.75-1.25	0.2-0.4	>25	0.5-0.7
LCZ 5 Open mid-rise	0.3-0.75	0.2-0.4	8-20	0.5-0.8
LCZ 6 Open low-rise	0.3-0.75	0.2-0.4	3-8	0.6-0.9
LCZ 7 Lightweight low-rise	1-2	0.6-0.9	2-4	0.2-0.5
LCZ 8 Large low-rise	0.1-0.3	0.3-0.5	3-10	>0.7
LCZ 9 Sparsely built	0.1-0.25	0.1-0.2	3-8	>0.8
LCZ 10 Heavy industry	0.2-0.5	0.2-0.3	5-15	0.6-0.9
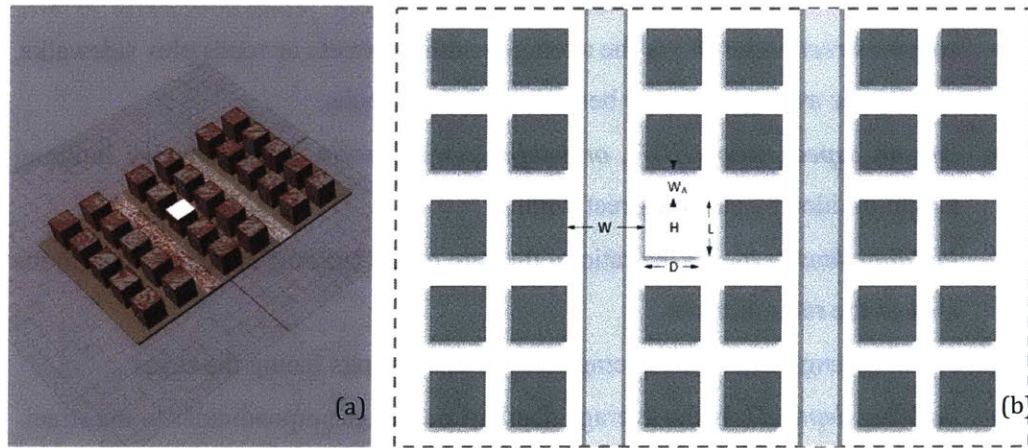
Figure 3.2 A generic urban neighborhood for the parametric analysis in the Rhino® interface. (a) perspective view; (b) top view

3.2.2 Parametric design of experiments and building energy simulations

Urban morphology comprises a set of parameters that describe the urban context and, consequently, impact building energy demand. To better understand the impact of these factors, we use a parametric approach called design of experiments (DOE), which generates individual cases with different combinations of parameters *(66)*. Usually, experiments are planned in a way that redundant observations can be eliminated without any loss of representativeness, reducing the number of runs needed to provide information about the major interactions between the variables. As a result, the relationship between the response variables of interest and the design variables can be studied using sensitivity analysis, the response surface method, or other machine learning techniques.

Definition of urban morphological parameters (input design variables)

To properly perform DOE in this study, we start by identifying the input variables and the response parameters of interest. In the literature, the quantitative description of urban morphology usually involves a number of morphological parameters, which can be calculated for any given urban neighborhood or an entire urban area:

- *building height (H)* is the average height of buildings within the reference site. It can be estimated from the parameter *number of storeys* in some databases.
- *canyon street width (W)* is the average width of streets or roads plus sidewalks, usually the average distance between building blocks.
- *canyon aspect ratio (H/W), or height-to-width ratio,* is the average building height divided by canyon street width.
- *building density (ρ_b)* is the ratio of the sum of the building footprint areas to the area of the reference site.
- *building length (L)* is the average length of buildings facing the street.
- *building depth (D)* is the average depth of buildings perpendicular to the street.
- *shape factor, or surface-to-volume ratio (S/V),* is the ratio of building external surface area (facades and roof) to the total volume of buildings.

In addition to the parameters defined above, there are a few other pavement-relevant morphological indicators:

- *alley width (W_A)* is the distance between buildings within a building block, usually used for parking space, walkways, or vegetation.
- *pavement density (ρ_p)* is the ratio of pavement areas to the site area.
- *façade density (ρ_f)* is the ratio of building façade area to the site area.

Fractional factorial design

In this study, we first explore four key input parameters that are considered expert judgement to be associated with pavement albedo and its impact on BED based on expert judgement: *building height (H), canyon aspect ratio (H/W), building density (ρ_b)* and *building length* (L). For each input variable, five levels are defined that represent the range of each variable as specified for each LCZ in Table 3.1. If computational cost were not a constraint, one would try all possible combinations of a full factorial design, which is $5^4 = 625$ runs. However, in the event of limited computational resources, a fractional factorial design method is employed, which defines the experimental sets consisting of a carefully chosen fraction of the experiments defined by a full factorial method. Such fraction is chosen so as to exploit the sparsity-of-effects principle capable of providing representative information about the most important effects related to the problem, while using a reduced fraction of the effort of a full factorial design in terms of experimental runs and computational resources. For this analysis comprising 10 LCZs, a full factorial design would have 625*10 = 6,250 neighborhood configurations in total for one location. Our experimental design is a fraction of the full design, that consists of 296*10 = 2,960 runs (296 configurations for each LCZ).

Radiation and energy simulation with Ladybug & Honeybee – calculating ΔE_R

Incident shortwave radiation

Ladybug and Honeybee connect Grasshopper® to validated simulation engines such as EnergyPlus™, RADIANCE, DAYSIM and OpenStudio® for building energy, comfort, daylighting and lighting simulation *(64)*. They are powerful and highly-optimized

modeling plugins for Rhino with Grasshopper. It has the capability of effectively calculating daylight metrics (using the RADIANCE engine) and energy consumption (using the EnergyPlus™ engine). The thermal components collect geometry, material, and schedule information associated with a building, and performs a full yearly thermal dynamic simulation. As a result, annual energy consumptions for heating and cooling are provided.

In both the radiation and the energy simulations, pavements are treated as external shading surfaces so that incident shortwave radiation received by the surfaces and reflected from them can be captured. The albedo of the pavement surfaces can be modified, so the changes in incident shortwave radiation and consequently BED due to such changes can be estimated by comparing the simulated result from a baseline scenario ($\alpha = 0.1$) with that from an increased-albedo scenario ($\alpha = 0.3$).

Longwave radiation estimation

Longwave radiation has been a challenge for building energy performance modeling at urban-scale. It depends on both geometric measures, such as the view factor between surfaces, and the temperatures of surfaces, including roofs, facades and grounds. Traditional building energy simulation tools developed for individual buildings are generally unable to capture all the interactions between building surfaces and the surrounding urban environment. For example, EnergyPlus™ calculates longwave radiation as thermal radiation transfers between building surfaces and air, sky and ground with arbitrary temperature, while neglecting transfers among building surfaces and the fact that all surface temperatures change simultaneously, including those of ground surfaces (U.S. Department of Energy 2015) *(67)*.

In this analysis, longwave radiation is simulated with the EnergyPlus™ engine in Honeybee, so it inherits the same limitations. However, based on a simple estimation we showed that the change in thermal radiation exchange between building surfaces due to pavement albedo change is two orders of magnitude smaller than that between air/sky/ground and building surfaces. In addition, instead of using an arbitrary ground

temperature, the air temperature simulated using UWG is used for ground temperature. The error on longwave radiation introduced by this assumption is only 5% to 10%, which is acceptable given the impact of longwave radiation is smaller than that of the incident shortwave radiation.

UHI/microclimate/ambient temperature simulation with UWG – calculating ΔE_T

Urban Weather Generator (UWG) is an urban design simulation tool that provides climate-specific temperatures for cityscape geometry and land use change *(68)*. It estimates the hourly urban canyon air temperature and humidity based on weather data from a rural weather station. The model takes input parameters that describe urban morphology, geometry, and surface materials, which makes it suitable for studying the impact of changing surface albedo on urban microclimate under different urban settings. The output from UWG is a modified weather file (.epw) that captures UHI effects and is compatible with many building performance simulation programs, including EnergyPlus™. The tool has been tested for several urban areas and can satisfactorily estimate urban temperatures in different climates, weather conditions, and urban configurations *(69)*. The performance of UWG is comparable to a more computationally expensive mesoscale atmospheric model *(70)*.

For this study, input parameters for UWG about urban morphology and surface properties, including mean building height, building density, canyon aspect ratio, etc., are extracted from the 3D urban geometries prepared in Rhino®. The model is run with an increased pavement albedo, and the output weather file is then imported back to the EnergyPlus™ module in Honeybee. The difference in BED between the baseline scenario with the original weather file and the scenario with the modified weather file is calculated as the indirect impact of increasing pavement albedo due to changes in ambient temperature, denoted as ΔE_T.

3.2.3 Meta-models for predicting ΔE ($\Delta E_R + \Delta E_T$) due to $\Delta \alpha$

Due to the constraints with computing power and time, it's not feasible to generate every single building geometry in an urban neighborhood and simulate the energy

consumption individually, and therefore a statistical meta-model is needed. From the DOE, changes in BED (ΔE) due to a 0.2 increase in pavement albedo ($\Delta \alpha = 0.2$) are simulated and recorded for the experimental design of 5,920 neighborhood configurations. In addition to the four input variables, two other dimensionless parameters, i.e., shape factor (S/V) and façade density (ρ_f), are also calculated for each neighborhood geometry based on the four known variables. These two dimensionless parameters, plus the *canyon aspect ratio* (H/W) and *building density* (ρ_b), are then used to build the statistical meta-models. They are chosen as the model predictors because each of them has an impact on pavement albedo-induced BED from different perspectives. Building density (ρ_b) and façade density (ρ_f) directly determine the area of buildings and building walls affected by the increase of albedo, thus the changes in the amount of incident radiation received and reflected from the pavements. They also impact the changes in canyon temperature. Canyon aspect ratio (H/W) affects the amount of solar radiation incident on the canyon floor, as higher buildings and narrower canyon results in more shadings and less incident radiation. Shape factor (S/V) has an influence on the effect of ambient temperature change on BED.

Response variables for the meta-models are the changes in heating BED and cooling BED, respectively, resulting from the 2,960 simulations, taking into account the effects of both incident radiation and ambient temperature. We evaluated various machine learning models to fit the data, including multiple regression, random forest regression, support vector machine, and neural networks. For each LCZ, these model forms were tested using the simulated data and the one with the best fit was identified. 10-fold cross validation is applied to avoid overfitting of the model. Neural networks were found to predict ΔE due to $\Delta \alpha$ with relatively good accuracy. The root mean square error (RMSE) and R-squared of the meta-models for the 10 LCZs in the case of Boston and Phoenix are summarized in Table 3.2, and Figure 3.3 is a validation plot showing actual vs. predicted ΔE from one of the meta-model fitting results.

58

Table 3.2 Root mean square error (RMSE) and R-squared of the meta-models for Boston and Phoenix created using neural networks

Local climate zone (LCZ)	Boston		Phoenix	
	RMSE	**R-squared**	**RMSE**	**R-squared**
LCZ 1	1.45	0.98	0.83	0.92
LCZ 2	0.10	0.98	0.09	0.98
LCZ 3	0.27	0.98	0.23	0.95
LCZ 4	0.21	0.96	0.52	0.95
LCZ 5	0.12	0.98	0.45	0.96
LCZ 6	0.05	0.98	0.35	0.98
LCZ 7	0.19	0.97	0.27	0.98
LCZ 8	0.09	0.92	0.66	0.97
LCZ 9	0.05	0.95	0.18	0.97
LCZ 10	0.28	0.96	0.22	0.98
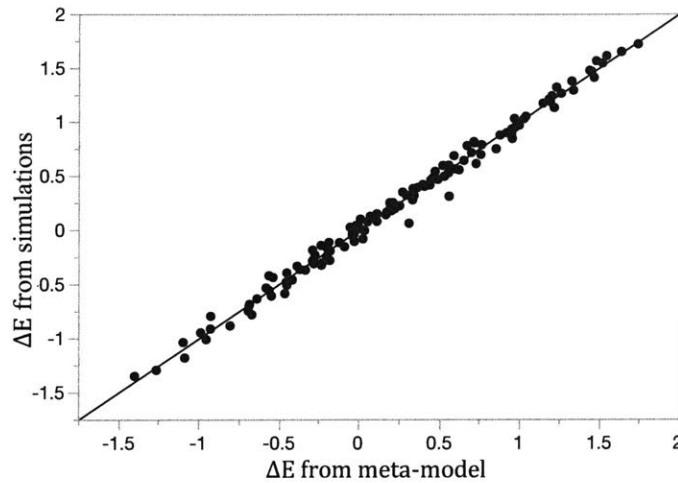
Figure 3.3 Residual plot from the meta-model fitting result for LCZ 1 in Boston

3.2.4 Application to realistic neighborhoods with GIS data

GIS data is widely used in spatial analysis and urban planning to support decision-making. Usually, GIS building information for a city is stored in vector or raster data in shapefile format. By overlaying layers of spatial boundaries, such as zip codes and census tracts, morphological characteristics can be calculated at different scales. For the cases studied here, shapefiles containing building information of Boston and Phoenix were obtained from MassGIS (Bureau of Geographic Information) *(71)* and the Arizona State University (ASU) Library Map and Geospatial Hub *(72)*, respectively. These shapefiles provide data on building footprints, building heights, building types, etc. In

59

addition, vector data containing primary road networks for Boston and Phoenix were contained in TIGER/Line® shapefiles from the U.S. Census Bureau *(73)*.

Building height, building density, road width, and building length are first aggregated at the census tract level using a GIS processing program called QGIS®. An LCZ is assigned to the census tract using the definitions in Table 3.1. For each census tract, the averaged building and road data are used to estimate the four dimensionless input parameters for the meta-models: canyon aspect ratio (H/W), shape factor (S/V), building density (ρ_p), and façade density (ρ_f). Applying the meta-models for different LCZs, changes in BED (heating and cooling) per square meter of pavement modified due to a 0.2 increase in pavement albedo are computed for every census tract.

Input parameters are also calculated at the individual building level in order to explore the impact of higher resolution analysis, where canyon aspect ratio (H/W) and shape factor (S/V) pertain to each building, instead of using the census tract aggregated values. Building density (ρ_b) and façade density (ρ_f) are estimated for the neighborhood where the building of interest is located, which is defined as a circle with the building as the center and a radius of 300 meters. Similarly, LCZs are assigned and changes in BED for each individual building are estimated using the meta-models.

3.3 Results and Discussions

3.3.1 DOE results and discussions

Changes in cooling and heating demands due to both incident radiation and ambient temperature effects as a result of increasing pavement albedo by 0.2 are simulated using the integrated model and recorded simultaneously. Apart from the four input variables pertaining to urban morphology, all other parameters related to the thermal properties of the buildings and the context are fixed, including the climatic conditions. A list of the parameters can be found in Table A1 in the APPENDIX A. To allow for direct comparisons of all different neighborhood configurations and their theoretical building energy demand, the climate conditions are set to that of the city under consideration and

60

the building construction is kept constant throughout (for the case of Boston, for example, buildings are set in Honeybee to values meeting ASHRAE standards 90.1-2010 *(74)* for climate zone 5A in Honeybee), leaving only urban morphology itself as the changing variable. Therefore, the effect of the physical dimensions of buildings and their layout at a larger scale on BED due to pavement albedo change becomes measurable.

Influence of canyon aspect ratio (H/W) and building density (ρ_b)

Results from the DOE show that canyon aspect ratio and building density both have a significant effect on BED due to changes in pavement albedo, but their impacts on cooling demand and heating demand are different. Figure 3.4 shows that the change in cooling demand first increases slightly with the increase of canyon aspect ratio, but decreases quickly after *H/W* reaches around 0.94. When the aspect ratio is small (<0.94), it resembles a wide canyon, where buildings are far apart and the average building height is small. Any modification on pavements is likely to have little or no impact on surrounding buildings. However, as the canyon aspect ratio continues to increase after 0.94, there is a greater average height of the buildings compared to the distance between them, which means more shadings cast on other buildings' roofs and facades. This in turn reduces the incident radiation received on building surfaces. The results is consistent with the solar radiation behavior expected in urban configurations. On the other hand, heating BED decreases as pavement albedo increases, so the changes are negative, indicating savings from heating. Such savings decrease as *H/W* increases because in narrow urban canyon with a higher aspect ratio, building surfaces receive less incident radiation due to obstruction. Furthermore, reduced ambient temperature due to increased pavement albedo tends to offset some of the heating benefits from increasing pavement albedo.

In this experimental design, building density (ρ_b) is correlated with canyon aspect ratio (*H/W*) to some extent, but its impact is less pronounced than that of canyon aspect ratio. The reason is that the reference site in this analysis not only consists of building footprints and pavements, but also the area in between buildings other than primary

roads. Higher canyon aspect ratio does not necessarily correspond to greater building density, as the alleys between buildings can be large too. Therefore, as shown in Figure 3.4, changes in cooling BED due to pavement albedo slightly reduce with ρ_b while changes in heating BED increase as ρ_b increases.
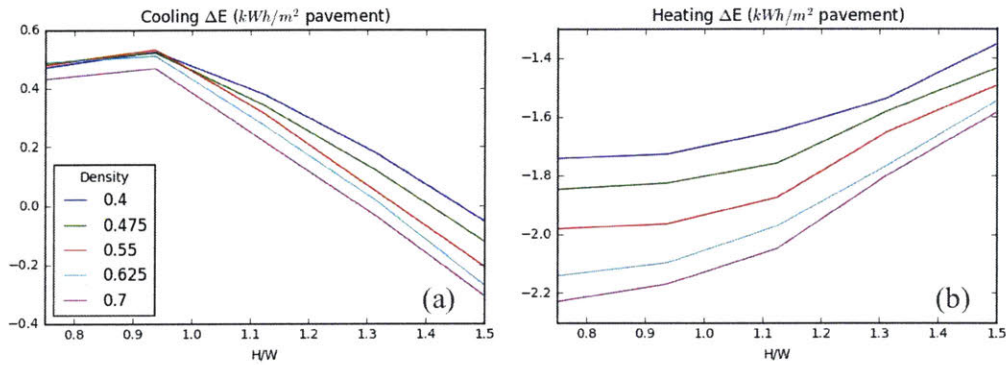
Figure 3.4 Changes in cooling demand (a) and heating demand (b) for Boston due to 0.2 increase in pavement albedo for samples with different values of canyon aspect ratio (H/W) and building density (ρ_b)

Influence of shape factor (S/V)

Shape factor, or surface-to-volume ratio (*S/V*), is a measure of building compactness. It has been considered as one of the building attributes that plays a significant role in building thermal exchanges *(75)*. Generally, increasing surface-to-volume ratio positively affects the energy demand in buildings. The larger the surface of the envelope, as opposed to the built volume, the more reflected radiation could be received by building facades, which represents greater solar heat gains to buildings. However, in this analysis, the response variable of interest is the change of BED ΔE (including both ΔE_R and ΔE_T) due to pavement albedo, which, as shown in Figure 3.5, is decreasing (absolute value) as shape factor increases. This is because the reduction in ambient temperature has a greater effect on less compact buildings (larger heating or cooling volume) given that the area of building façade facing the modified pavement is the same. As a result, the impact of changing pavement albedo is more significant for buildings with lower shape factors.

62
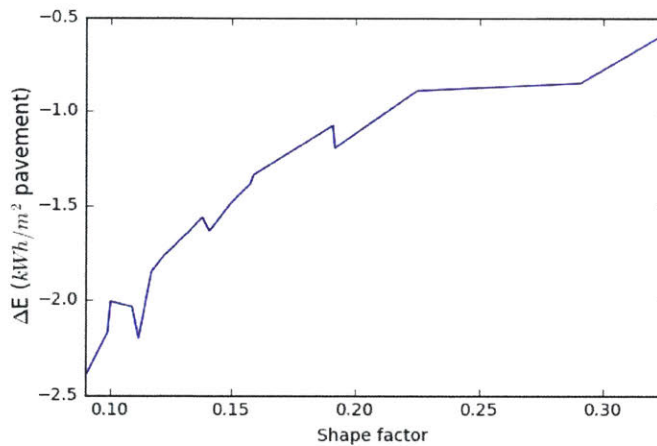
Figure 3.5 Changes in total BED (ΔE) for Boston due to 0.2 increase in pavement albedo for samples with different shape factors

Incident radiation vs. ambient temperature

It should be noted from Figure 3.4(a) that the changes in cooling BED due to increased pavement albedo are positive when *H/W* is small, indicating net burdens on cooling BED. However, when *H/W* is big or in densely built neighborhood, the value becomes negative, indicating BED savings from cooling. The switch of sign reveals a trade-off between the two mechanisms: incident radiation and ambient temperature, which can be explained by the underlying physics. In EnergyPlus™, energy demand is calculated by solving a series of heat balance equations on building envelope, indoor and outdoor air.

On the building external wall, the heat balance can be written as:

$$q_{sw} + q_{lw} + q_{cv} - q_{cd} = 0 \tag{3.1}$$

where

q_{sw} is the shortwave radiation, including direct, reflected and diffuse solar radiation

q_{lw} is the longwave radiation from the environment, including sky, air and the ground

q_{cv} is the convective flux from the environment

q_{cd} is the conductive flux through the wall

63

Increasing pavement albedo has a direct effect on q_{sw}; more solar radiation is reflected from the pavement. It also causes ambient air temperature to reduce, so does the ground temperature. As a result, both the longwave radiation q_{lw} and the convective flux q_{cv} from the environment decrease. The net balance of the increased q_{sw} and decreased $(q_{lw} + q_{cv})$ determines the direction of conductive flux q_{cd} through the wall, ultimately affecting the heat gain and energy demand indoor. The relative magnitude of the shortwave q_{sw} and the longwave radiation q_{lw} depends on urban morphology, which is why the sign change is observed for changes in cooling BED in Figure 3.4(a).

3.3.2 Case study results and discussions

To demonstrate the proposed methodology, two cities, Boston and Phoenix, were chosen as test cases, representing a cold and hot climate, respectively. Data on urban morphology characteristics and building dimensions were extracted from geographic information system (GIS) databases and aggregated at different scales. Simulation-based meta-models were then used to predict changes in BED (normalized to the area of pavement modified) due to a 0.2 increase in pavement albedo at two scales: the census tract level and the building level.

Census tract level

The GWP impact of increasing pavement albedo by 0.2 on BED is calculated from changes in cooling and heating BED, multiplied by corresponding CO_2 emission factors, respectively. The emission factors for electricity come from the 2016 Emissions & Generation Resource Integrated Database (eGRID) *(76)*. For NEWE New England subregion where Boston is located, the non-baseload emission rate is 980.5 lbs CO_2-e/MWh (0.445 kg CO_2-e/kWh), and for WECC Southwest where Phoenix is located the rate is 1391.2 lbs CO_2-e/MWh (0.631 kg CO_2-e/kWh). The emission factor of natural gas for heating is 0.181 kg CO_2/kWh based on US Environmental Protection Agency (EPA)'s Greenhouse Gases Equivalencies Calculator *(77)*. The results for Boston and Phoenix are calculated over a 50-year analysis period and shown in Figure 3.6 and

64

Figure 3.7, respectively, at the census tract level. The results of the LCZ categorization for the two cities are also shown in Figure 3.6(a) and 3.7(a), respectively. Building density decreases from LCZ 1 (compact high-rise) to LCZ 9 (sparsely built). It can be seen from the maps that increasing pavement albedo exerts negative impacts for mid- to high-density neighborhoods, creating a net burden on BED due to the greater influence of increased incident radiation reflected from the roads and heat trapping among buildings. In low-density residential areas, however, the negative effects imposed by increased solar radiation gains tend to be balanced by the benefit of reduced ambient temperature from the cooler pavements. The net effect highly depends on urban morphology and microclimate.
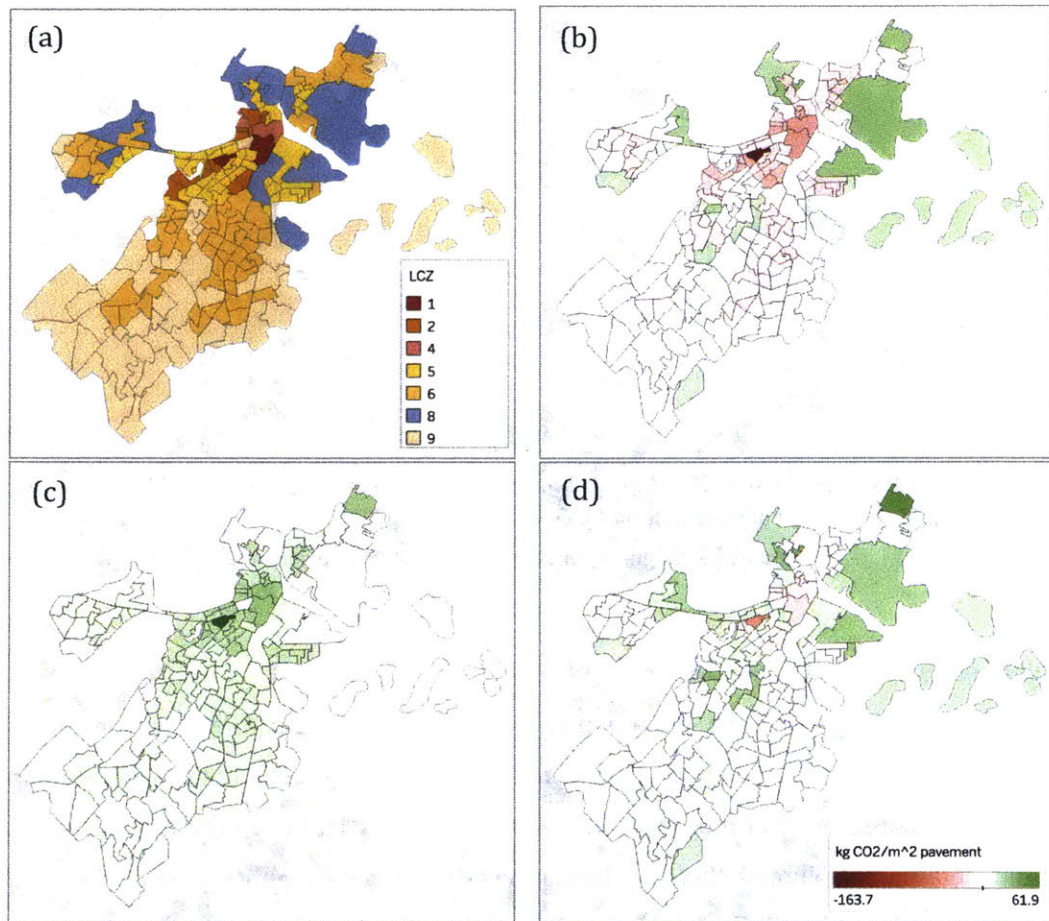
Figure 3.6 GWP savings from BED due to a 0.2 increase in pavement albedo in Boston over a 50-year analysis period. A negative number indicates a GWP burden. (a) LCZs, (b) cooling, (c) heating and (d) total BED. Figures generated in Tableau® software

65
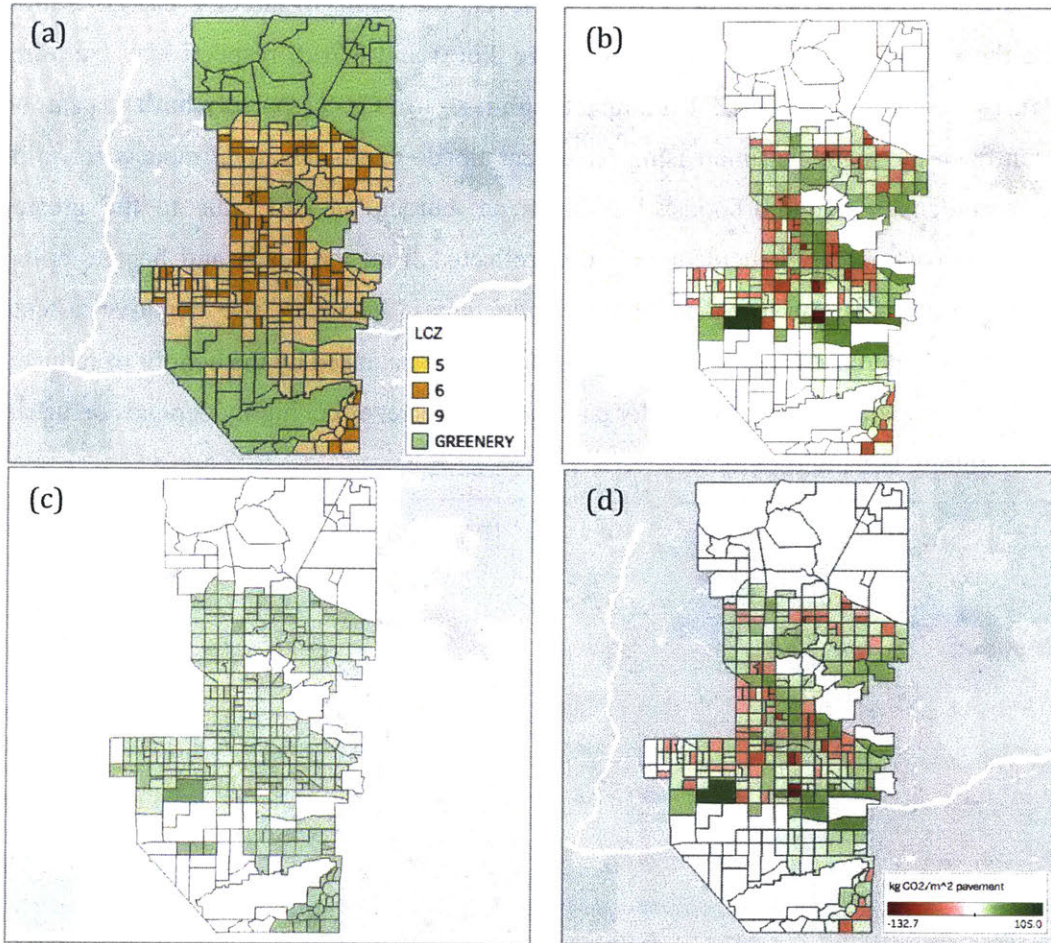
Figure 3.7 GWP savings from BED due to a 0.2 increase in pavement albedo in Phoenix over a 50-year analysis period. A negative number indicates a GWP burden. (a) LCZs, (b) cooling, (c) heating and (d) total BED. Figures generated in Tableau® software

Building level

Figure 3.8(a) is part of the Boston map showing the 50-year GWP savings from increasing pavement albedo by 0.2 at the individual building level. For any building in the GIS database, the four morphological parameters were extracted and used as inputs to the meta-model. Though there are limitations when directly applying meta-models at the individual building level, such granular results provide a first-order approximation of the GWP savings or burdens due to the increase in pavement albedo. By identifying target neighborhoods with potential interest in implementing reflective pavement

66

strategy, the proposed method allows for closer scrutiny of the potential impacts on buildings around the treated pavement segments. Figure 3.8(b) is a picture of the neighborhood blocks marked with a red circle. The pavement segment of interest is Federal Street between Milk Street and Matthews Street. There are two main lanes and two shoulders. The length of the segment is 929ft (283m). Reading the meta-model results from the map on Figure 3.8(b), GWP saving from increasing the albedo of the pavement segment in this neighborhood is about 19.17 kg CO_2 per square meter of pavement (by summing up the numbers in the figure). Multiplying this number by the area of the pavement segment (283m×14.6m), the total GWP saving for this selected neighborhood is 79.2 Mg CO_2 over 50 years. Further simulation with the exact dimension and context will improve the accuracy of the estimation and is thus recommended when conducting a more detailed assessment.
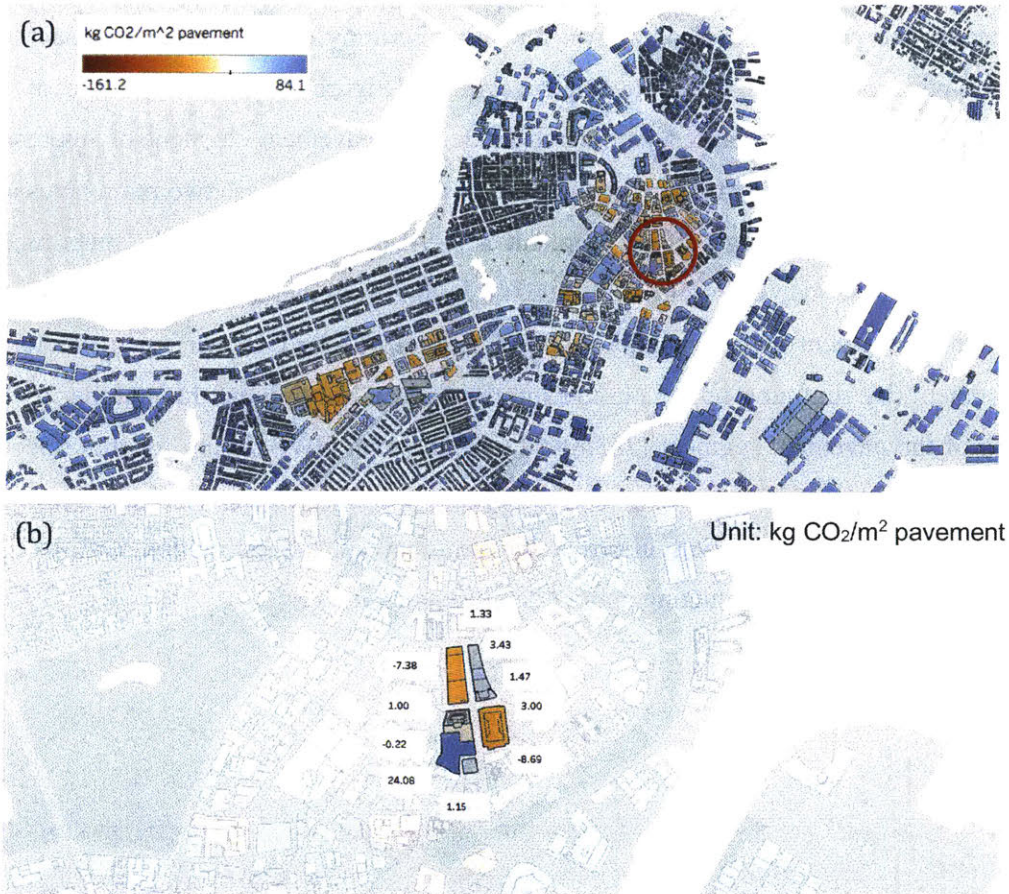
Figure 3.8 GWP savings from BED at building level due to a 0.2 increase in pavement albedo in Boston over 50 years (a negative number indicates a GWP burden). (a) A snap shot showing Boston downtown and Back Bay area with the neighborhood of interest marked by red circle; (b) GWP saving results for each building in the selected neighborhood

3.4 Conclusions

In this chapter, two research questions were answered through parametric analysis and case studies:

- What is the mechanism that drive changes in BED due to the pavement albedo enhancement?

- What are the contextual factors that significantly affect BED due to pavement albedo changes?

68

An innovative methodology is proposed for modelling urban-scale building energy demands (BED), taking into account various contextual factors. Experimental design is carried out to better understand the influence of urban morphology on BED due to pavement albedo changes. The trade-off between two mechanisms: incident radiation and ambient temperature is investigated and discussed based on simulation results. Which mechanism is dominant depends on a number of contextual factors. Overall, the hypothesis that urban morphology and pavement albedo have significant impacts on BED is confirmed. Several morphological parameters are identified as the most influential factors. Among those parameters, canyon aspect ratio and building density are found to have greater influence on the amount of incident radiation receiving by building surfaces, correlating with the solar heat gains of building thus the BED. The surface-to-volume ratio also correlates well with BED, but shows a greater ambient temperature effect than that of direct incident radiation. Results from the experimental design and the case study of Boston and Phoenix validate our hypothesis that the impact of pavement albedo change on BED is context dependent. Increasing pavement albedo usually create burdens on BED for densely-built neighborhoods while low-density neighborhoods are more likely to benefit from more reflective pavements.

Therefore, it is recommended that urban morphology and microclimate should be taken into account by designers and policy makers in urban planning and decision makings for improving building energy efficiency and mitigating CO_2 emissions at an urban scale. The effectiveness of increasing pavement albedo, as one of the potential cool pavement strategies, should be evaluated under specific urban contexts at a neighborhood level making use of GIS data. In addition, a more comprehensive evaluation of the impact of reflective pavements is necessary, taking into account other phases and components in a pavement's life cycle. Further research on the impact of building properties on BED as well as data collections on the evolution of pavement albedo would improve the robustness of the model for supporting sustainable pavement designs.

CHAPTER 4 PAVEMENT LIFE CYCLE ASSESSMENT WITH CONTEXT-SPECIFIC IMPACTS OF PAVEMENT ALBEDO

4.1 Introduction

Life cycle analysis (LCA) provides a comprehensive evaluation of the environmental burdens from a product or service by quantifying the environmental effects of a product throughout its life cycle. In LCA, the inputs (such as energy and resource consumption) and outputs (such as emissions) are identified and inventoried over the product's entire life cycle, which usually includes the material production, transportation, construction, use, and end-of-life. LCA has been introduced to the field of pavement industry in the past decade *(78–80)*. While guidance and standards have been developed for conducting pavement LCA, it has not been widely implemented for supporting environmentally conscious pavement designs, partially due to the existing limitations in sub-models for quantifying the impacts of pavement in the use phase *(2)*. In the past, the impacts of pavement albedo in the use phase were often ignored or quantified using very simple models in pavement LCA, which were not location-specific and exhibit huge uncertainties. Gilbert et al (2017) developed a pavement LCA tool to evaluate the use-stage environmental effects of pavement, but it is limited to albedo impacts and excludes other important use-phase components, such as the influence of pavement-vehicle interaction (PVI) on fuel consumption *(81)*. No one has quantified the impacts of RF and BED due to pavement albedo under different contexts. The net effect of these two impacts in the context of pavement LCA also remains unknown.

Paved surfaces account for 30 to 40 percent of all surface areas in U.S. urban areas, including roadways, sidewalks, parking lots, and hardscape playgrounds *(82)*. Conventionally, most paved surfaces (over 80 percent) are constructed with asphalt concrete, which has characteristically low albedo *(83)*. Low albedo contributes to the surface warming of asphalt concrete, leading to the so-called "Urban Heat Island" (UHI)

effect. The UHI effect accelerates smog formation *(4)*, threatens the health and well-being of urban residents, and increases air conditioning energy demand and thus greenhouse gas (GHG) emissions *(84)*. To improve public health and reduce GHG emissions, some cities in California began to adapt to changing climate by implementing "cool" roofs and "cool" pavement strategies. Studies have shown that raising pavement albedo lowers the surface temperature, which in turn mitigates the UHI and reduces energy demands *(85)*. Rosenfeld et al (1998) showed that the contribution of cool pavements to lower outdoor air temperatures would reduce peak power demand by 100 MW and save $6 to $18 million in annual air conditioning energy in the Los Angeles Basin *(4)*. Pomerantz et al (2015), however, estimated that the building cooling energy saving for a city-wide albedo increase of 0.20 is less than 2 kWh per year per square meter of city surface modified *(86)*.

Recognizing the potential for reflective (high albedo) pavements to reduce GHG emissions, mitigate UHI effect, and improve air quality, in this study we developed several case studies to examine the life cycle impacts of reflective pavements in selected urban neighborhoods in Boston and Phoenix. In particular, within the use phase, both the radiative forcing (RF) and the building energy demand (BED) impacts associated with pavement albedo are quantified, including the "direct" impact of pavement albedo – the influence of local road albedo on the energy demand of surrounding buildings exposed to sunlight reflected from the road, and the "indirect" effect of pavement albedo – the influence of pavement albedo on air temperature and associated building energy demand with that air temperature change. The direct effect of pavement albedo change is simulated with EnergyPlus™ to account for external surface modifications. The indirect effect of air temperature change due to pavement albedo change is estimated by applying an urban climate simulator, Urban Weather Generator (UWG). The air temperature changes are then included in the building energy simulations. The direct and indirect effects of increasing pavement albedo usually have different or even contradictory impacts on building energy demand, depending on the climate conditions and the urban geometry where the pavement is located. Since the potential benefits of cool pavements can vary widely by location, and substituting cool pavement materials

for conventional materials may even produce undesired effects in certain instances, pavement life cycle assessment with location-specific models for pavement albedo is necessary for decision-makers to understand the life cycle environmental consequences of various pavement management options.

This Chapter applies the newly developed location-specific models for RF and BED presented in Chapter 2 and Chapter 3 to pavement LCA. The impact of context-specific factors, including location, urban morphology, shadings etc., are taken into account in both models. This work provides a comprehensive evaluation of the effectiveness of implementing reflective pavement strategies at a neighborhood scale and at an urban scale. It will be very useful for urban planners, transportation agencies or pavement designers to encourage sustainable pavement designs in order to meet the GWP mitigation goal.

4.2 Methodology

4.2.1 Probabilistic pavement LCA model

The datasets and the algorithms used to generate the LCA results were developed with complementary research efforts into pavement life cycle inventories, pavement-vehicle interaction, pavement albedo, and urban-scale building energy simulations. The full methodology can be found in Noshadravan et al. *(87)* and Xu et al. *(88)*, as well as Chapter 2 and 3 in this thesis, but a summary of the research efforts follows, with some key elements of the LCA model summarized here.

The scope of the model is presented in Figure 4.1. Of particular note is the use phase (as defined in the pavement LCA literature), which includes quantification of impacts from albedo, carbonation, lighting, roughness-derived pavement-vehicle interaction (PVI), and deflection-induced PVI. Our pavement LCA model can be used to calculate any number of life cycle impact assessment metrics, but in this study, we present results in terms of global warming potential (GWP) based on the emission factors provided by the Intergovernmental Panel on Climate Change (IPCC) *(26)*. The specific LCI data

sources and assumptions for all activities in the model are described in the APPENDIX B.
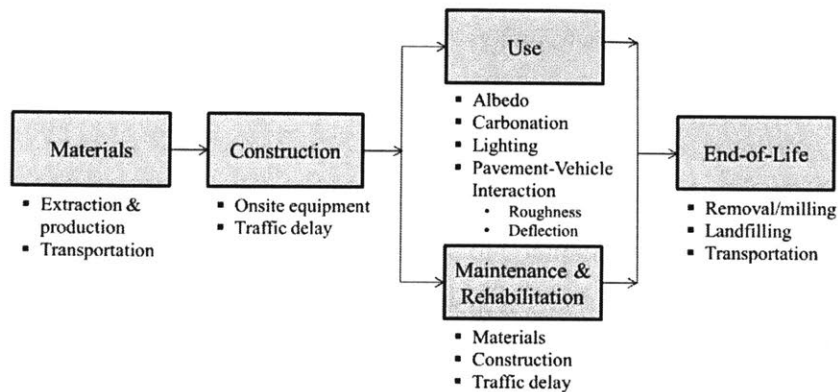
Figure 4.1 Scope and boundary of pavement LCA

Pavement-vehicle interaction (PVI) accounts for the excess fuel consumption in the vehicles on the road caused by the change in the structural and surface properties of pavements. It is important to emphasize that this is not the entire burden of fuel use, but rather the effect of pavement properties on the fuel economy of vehicles. Two major sources of PVI include fuel losses due to changes in roughness and fuel losses due to deflection of the pavement. The LCA model accounts for both roughness and deflection components. It is important to note that both the impact of maintenance on PVI and the improvement of vehicle fuel economy are taken into account in this model.

The deflection losses are calculated based on the model developed by Akbarian et al. *(2)*. The model uses a mechanistic approach to predict the deflection of the road over its lifetime as a function of the structural properties of the pavement. The predicted deflection can then be translated to the associated increase in the fuel loss relative to a fully rigid pavement. This is a novel model which has been calibrated to national highway performance values. Further extensions and refinements to the model continue and thus, an associated level of uncertainty was ascribed to the model predictions. To reflect this a significant level of uncertainty was ascribed to the predictions of this model. Roughness is characterized by the international roughness index (IRI). The prediction of IRI over time is extracted from output of the pavement design software, Pavement-ME, which implements the calculations specified by the Mechanistic-

74

Empirical Pavement Design Guide (MEPDG) *(89,90)*. The progressive change in the roughness relative to its value at initial construction is calculated and translated to the extra fuel consumption using the empirical model presented by Zaabar and Chatti *(91)*. Equation (4.1) and (4.2) show the calculations of the emissions from roughness and deflection induced PVI:

$$GWP_{IRI} = \sum_{t=1}^{T} \Delta IRI_t \times (\Delta AADTT_t \times K_{fc_{truck}} \times EF_{diesel} + \Delta AADT_t$$
$$\times K_{fc_{car}} \times EF_{gas}) \times t \tag{4.1}$$

where ΔIRI_t is the change in IRI within time interval t, $\Delta AADTT_t$ and $\Delta AADT_t$ are truck and car traffic during t, $K_{fc_{truck}}$ and $K_{fc_{car}}$ are the coefficients that translates ΔIRI into fuel consumption derived from Zaaba and Chatti's calibration of HDM-4 model, and EF_{diesel}, EF_{gas} are the GWP emission factors for diesel and gas.

$$GWP_{DEF} = \sum_{t=1}^{T} f_{truck}(E, k, h)_t \times \Delta AADTT_t \times EF_{diesel}$$
$$+ f_{car}(E, k, h)_t \times \Delta AADT_t \times EF_{gas}) \times t \tag{4.2}$$

where $f_{truck}(E, k, h)_t$ and $f_{car}(E, k, h)_t$ are fuel consumptions for trucks and cars in time t as functions of elastic modulus E, subgrade modulus k and pavement thickness h, calculated from MIT deflection model.

Uncertainty Characterization and Propagation

One particular merit of our pavement LCA model is that we employ a probabilistic approach, accounting for the uncertainties associated with the input data. A complete description of our probabilistic pavement LCA methodology can be found in Noshadravan et al *(87)*.

Pavement LCA depends on a variety of data that define a specific analysis. Given the scope and nature of life cycle assessment, significant uncertainty is associated with

much of that data. For the analyses presented here, probability distributions have been associated with most modeling parameters. These distributions were characterized either from available empirical data or expert estimates based on the ecoinvent guidelines *(92)*. This includes the parameters used to describe pavement design and maintenance, other LCI data, and the impacts of upstream processes (such as electricity generation or truck transportation). More information on the uncertainty characterizations for the parameters used in this study can be found in APPENDIX B.

Monte Carlo simulation is performed to propagate the parameter uncertainty into the estimated life cycle GWP using a computational LCA model we have developed. In each run of the simulation, a set of parameter samples are drawn from their corresponding distributions, and the life-cycle GWPs are calculated. The calculations are repeated N times, resulting in N realizations of GWP. From these realizations, the statistical characteristics of GWP can be estimated. The results presented here are based on 10,000 simulations for each scenario.

4.2.2 Pavement albedo models

The albedo of a pavement is characterized by a dimensionless number, which varies from 0 (fully absorbent) to 1 (fully reflective). The estimation of offset requires a baseline value of reflectivity with respect to which an equivalent carbon dioxide quantity is calculated. In this work we set the baseline value to 0.3, which roughly represents the average reflectivity of the earth. $\Delta\alpha$ is the change in albedo calculated with reference to a baseline albedo of 0.3. Ranges of albedo for difference pavement surface materials are summarized in Table 4.1. The CO_2 offsets due to RF and BED are calculated using the context-specific models developed in **Chapter 2** and **Chapter 3**.

Table 4.1 Albedos for different types of pavement surfaces

Pavement surface type	Ranges of albedo	Source
Conventional Asphalt Concrete (AC)	0.05 – 0.10 (new) 0.10 – 0.15 (aged)	ACPC (2002) *(93)*
Portland Cement Concrete (PCC)	0.35 – 0.40 (new) 0.20 – 0.30 (aged)	ACPC (2002)
White Cement Concrete	0.70 – 0.80 (new) 0.40 – 0.60 (aged)	ACPC (2002)
Reflective Coatings	0.50 – 0.80 (new) 0.20 – 0.30 (aged)	Levinson (2017) *(94)*

4.2.3 Reflective pavement designs and scenarios

Functionally equivalent flexible (asphalt in the top layer) and rigid (concrete in the top layer) pavement designs and maintenance schedules have been created using the AASHTO Pavement-ME software and associated MEPDG models by pavement engineers. The functional unit in all analyses is one center-lane mile of pavement. Details about the designs can be found in APPENDIX C, but the designed traffic and site conditions are summarized as followed:

Traffic:

Traffic load for Boston is obtained from city of Boston (https://data.boston.gov/dataset/traffic-related-data), at A Street north of Iron Street, which is represents typical local street in Boston, i.e. including two traffic lanes, two parking lanes and two bike lanes. Similarly, traffic load of a local street in the city of Phoenix is obtained from https://catalog.data.gov/dataset/phoenix-study. Average Annual Daily Truck Traffic (AADTT) is 1600 for two directions with a 3% compound annual increase.

Site conditions:

77

- Urban local roadway, two travel lane each direction.
- Traffic loadings: The AADTT two directions is 1600, assuming 50% in the design direction.
- Soil support: AASHTO class is A-2-5, coarse grained soil based on the national soil map developed by Arizona State University. The mean subgrade resilient modulus is 16,000 psi.
- Climate: The project sites are in Boston MA and Phoenix AZ, respectively.
- Reliability and performance criteria: national default of the program.
- AC failure criteria: International Roughness Index (IRI), total rutting, AC bottom-up fatigue cracking, and thermal cracking. Use levels recommended in MOP for each site and traffic level.
- PCC failure criteria: IRI, bottom-up and top-down transverse fatigue cracking, faulting. Use levels recommended in MOP for each site and traffic level.
- Material mix: Material mixes for asphalt and concrete pavements are consistent with local agency practices and pavement design life.

In order to understand the impacts of pavement albedo under the context of the full life cycle of pavements, this study investigates five pavement designs scenarios with different constructions or maintenance strategies for urban conditions, as shown in Table 4.2. Scenario 1 and Scenario 3 are the baseline PCC and AC designs, while the rest are reflective pavement designs, with different surface treatment techniques to increase the pavement albedo. Two urban contexts were considered for each design scenario outlined in the table: one in Boston, MA and one in Phoenix, AZ, representative of cold and hot climate. This leads to a total of 10 scenarios. The impact of local climate zone (LCZ) on the pavement LCA results is also investigated and discussed.

Table 4.2 Overview of reflective pavement design scenarios (PCC=portland cement concrete; AC=asphalt concrete; M&R=maintenance & rehabilitation)

Urban Road Design Scenarios	New construction	M&R	Aged albedo
1	PCC	Full depth repair	0.25
2	High-albedo PCC	Full depth repair	0.5
3	AC	Mill & fill AC overlay	0.1
4	AC + coating	Mill & fill AC overlay + reflective coating	0.25
5	AC + high-albedo coating	Mill & fill AC overlay + high-albedo reflective coating	0.5

4.3 Results and Discussion

4.3.1 Comparing different reflective pavement strategies

The first objective of this analysis is to compare different reflective pavement designs and understand the effectiveness of cool pavement strategies in GHG mitigation. Figure 4.2 presents the results of the pavement LCA for the five pavement design scenarios of 30-year design life and 50-year analysis period, with MEPDG-derived maintenance schedule, for the two selected cities.

It can be seen from the figure that reflective pavement surface materials exhibit great GWP savings as compared to their conventional counterparts. Among these reflective designs, PCC pavements with high-albedo materials has the lowest life cycle GWP impact. For the same new AC construction, pavements with high-albedo (0.5) coating exhibit the greatest GWP saving, which makes AC pavement designs with reflective coating an attractive option for reflective pavement designs if high-albedo can be easily achieved without costing too much. Ordinary coating for AC pavements with an albedo of 0.25 doesn't seem to improve the life cycle impact of AC pavements significantly.
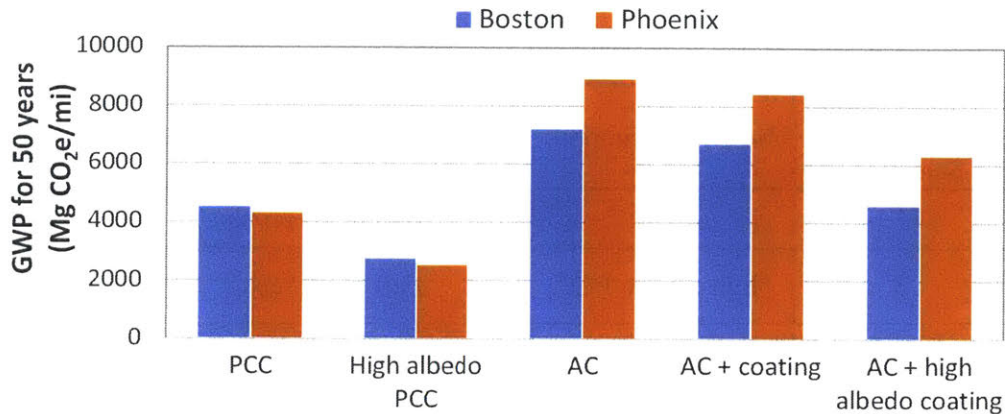
Figure 4.2 50-year life cycle GWP impacts for conventional PCC and AC designs and reflective PCC and AC designs in Boston and Phoenix

A breakdown of the life-cycle impacts for the five design scenarios in the context of Boston is shown in Figure 4.3. Two sets of scenarios are compared. Figure 4.3(a) is the breakdown of GWP for new constructions with initial constructions of AC and PCC, assuming no pavement has been installed or a complete rehabilitation is needed. Figure 4.3(b), on the other hand, assumes that AC pavement has already been in place, so PCC and AC overlay without initial construction are the two options being considered. Each color represents a life cycle component of a pavement design. From the figure, it is obvious that materials and construction contribute to a large percentage of total life cycle GWP impact for PCC designs. However, for AC designs, use phase impact, especially the excess fuel consumption from roughness and the impact of albedo, drives the total GWP. The relative magnitude of pavement albedo impact is smaller but can be comparable to that of the PVI impact in the use phase.
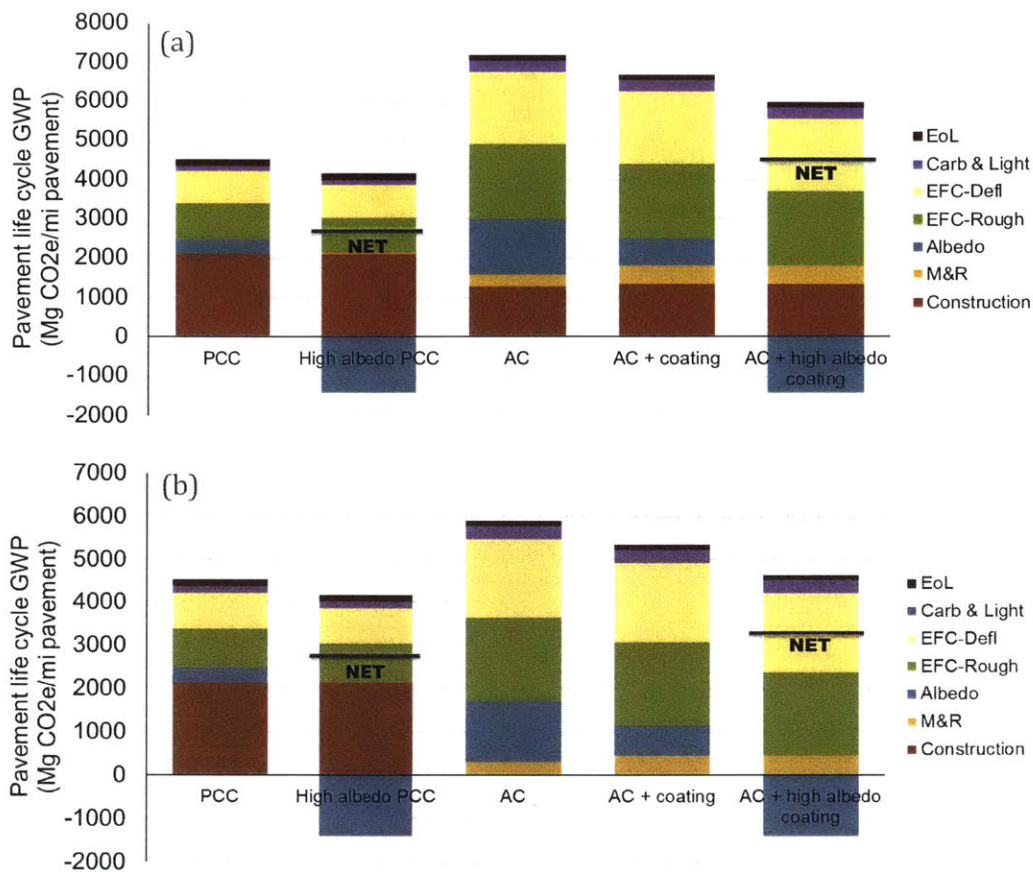
Figure 4.3 Breakdown of pavement life cycle GWP impact for conventional PCC and AC designs and reflective PCC and AC designs in Boston, assuming (a) new constructions including initial construction of AC and PCC, and (b) existing AC construction. Albedo impacts relative to baseline of average earth albedo (0.3). M&R=maintenance & rehabilitation; EFC= excess fuel consumption; Defl=deflection; Rough=roughness; Carb & Light= carbonation & lighting; EoL= end-of-life

4.3.2 Comparing different LCZs – effect of context

Location-specific models for quantifying the GWP impacts of increasing pavement albedo on BED and RF have been developed and applied to the city of Boston at census tract level. Figure 4.4 shows the 50-year net savings from BED and RF due to a 0.2 increase in pavement albedo for Boston, calculated from the context-specific models developed in Chapter 2 and Chapter 3. It can be seen from the map that most of the census tracts in Boston area would benefit from reflective pavements in terms of GWP savings, except several dense-built high-rise neighborhoods in the downtown area.
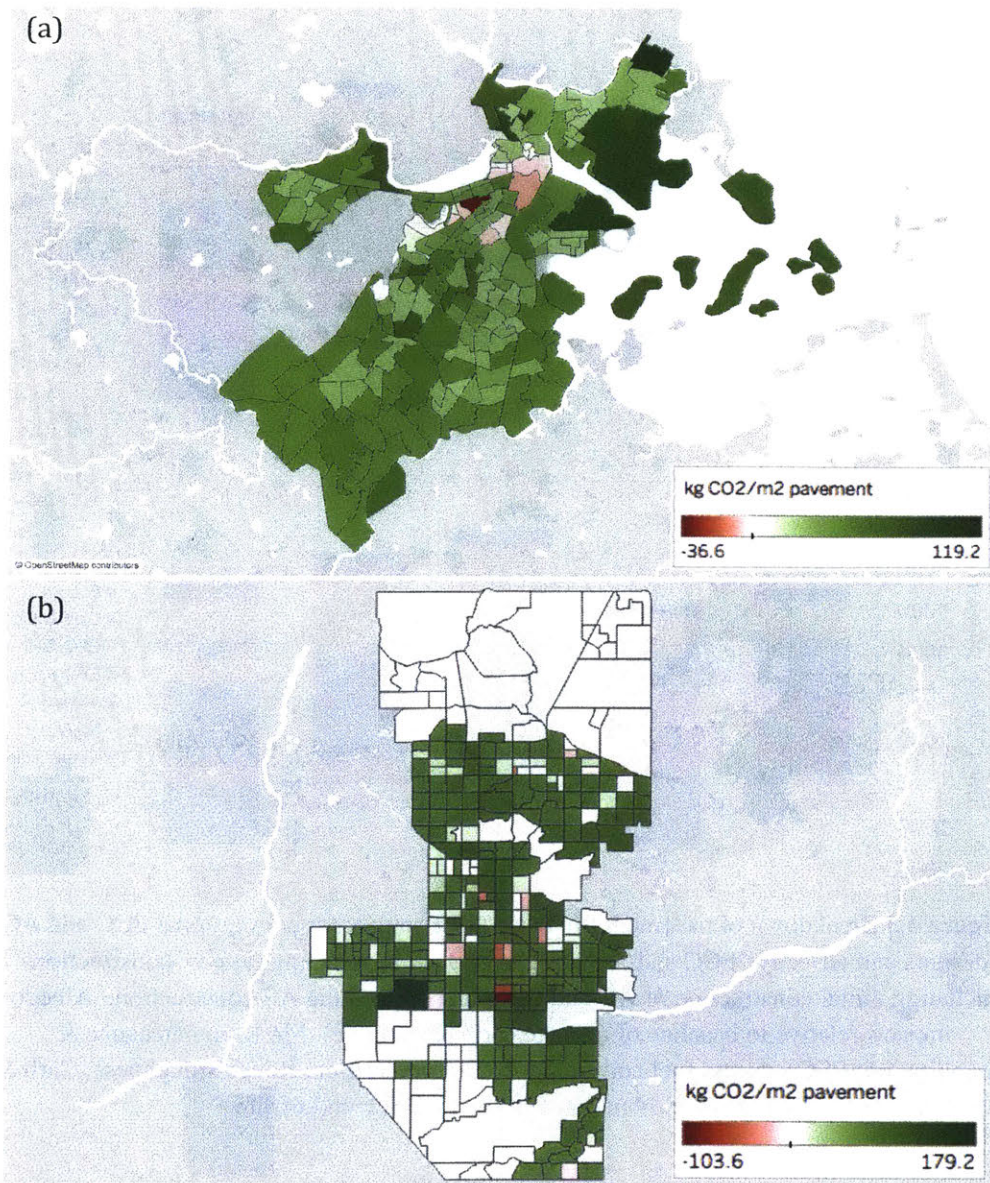
Figure 4.4 Net GWP savings from BED and RF due to 0.2 increase in pavement albedo in (a) Boston and (b) Phoenix for 50 years

When these albedo impacts are incorporated into pavement LCA, they can affect the pavement design decision. Since our pavement LCA model is developed using a probabilistic approach, uncertainties associated with the inputs are characterized and propagated into the results. Therefore, the analysis can be done probabilistically with Monte Carlo simulation. GWP for different designs are simulated 10,000 times for each census tract of the two cities, and the design that has the statistically significantly (more

than 8,000 times out of 10,000 runs) lowest GWP impact is selected as "Design-to-go", as shown in Figure 4.5. Whether initial construction is included or not, it is obvious that AC pavement is preferred in one of the most densely-built census tracts in Boston (denoted as "Back Bay") as life-cycle GWP impact of AC pavement is statistically lower than the other pavement designs. When we assume existing AC construction, high-albedo PCC pavement designs are desired in some dense neighborhoods, while in most low-density census tracts there is a statistical tie between PCC design and AC design with reflective coating, meaning that both PCC design and AC with coating may achieve the similar GWP saving benefit.
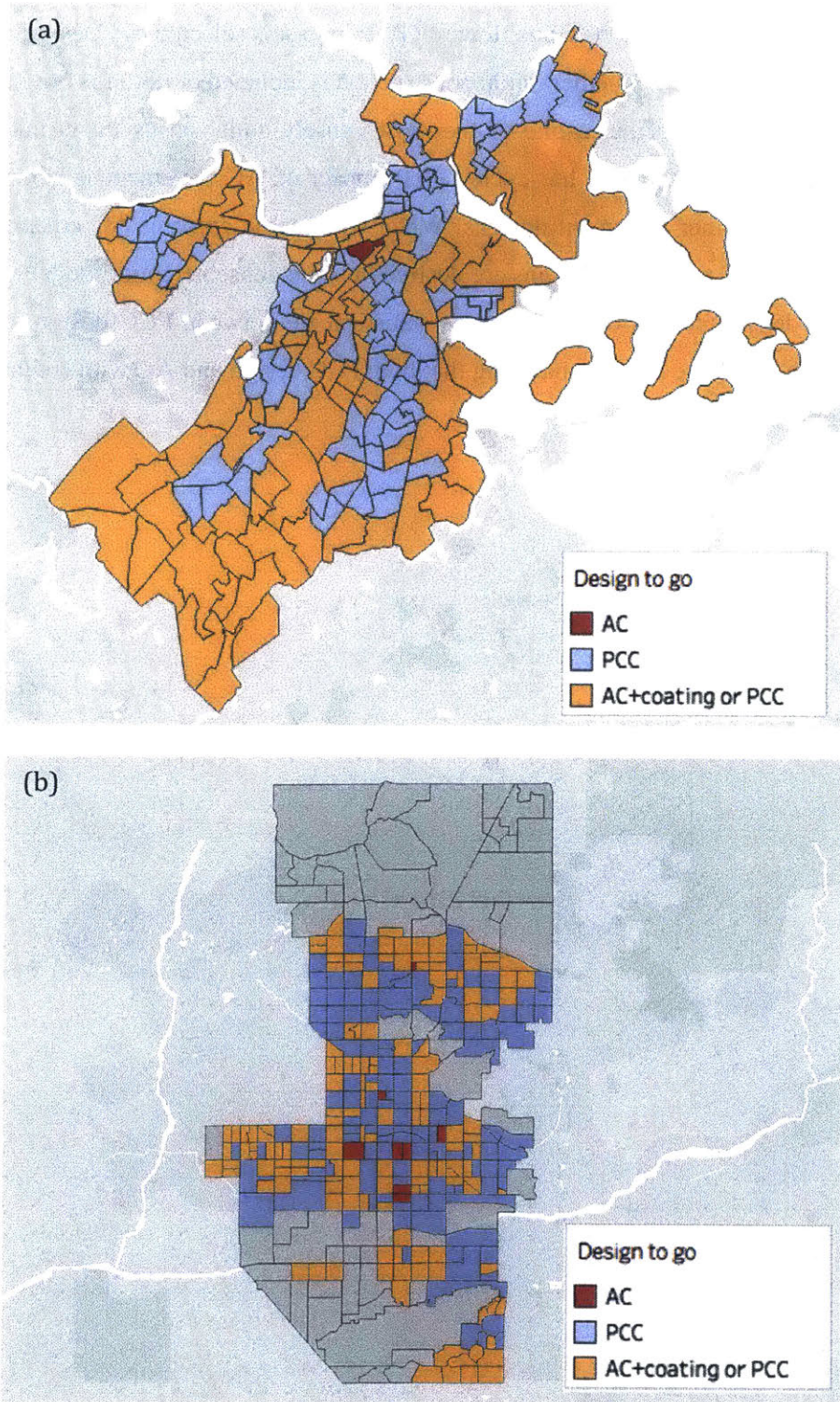
Figure 4.5 Best pavement design with lowest life cycle GWP impact for (a) Boston census tracts and (b) Phoenix census tracts

Life-cycle GWP impacts from 10,000 simulations for AC and PCC design scenarios in Boston are obtained and the differences between AC and PCC are computed for each run of the simulation. The histogram of the 50-year GWP savings ($GWP_{AC} - GWP_{PCC}$) is shown in Figure 4.6. Considering most of existing roads in Boston are made of asphalt, it makes sense to keep the roads in Back Bay as they are, and the rest of the roads can be converted to higher albedo roads to achieve GWP savings. We obtain the lane-miles of roads in each census tract of Boston and Phoenix, and calculate the percentage of total lane-miles that can be converted to reflective pavements according to Figure 4.5. If 32.1% of the roads were converted to PCC and 67.5% of them were converted to AC with reflective coating, the resulting average GWP savings from increasing albedo by 0.2 could be as much as 1,005 kton for 50 years. This is equivalent to 1.25% of the greenhouse gases (GHGs) emission from the transportation sector in Boston *(95)*.
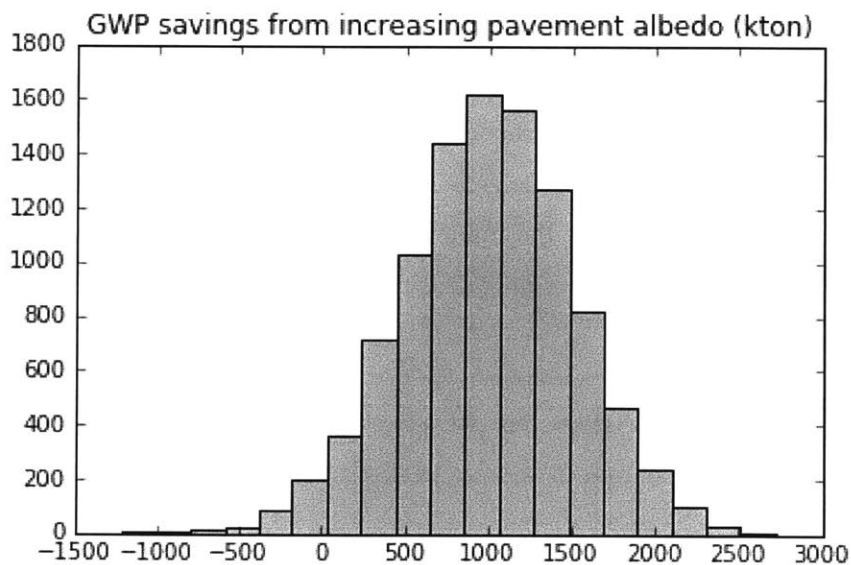
Figure 4.6 Histogram of the total GWP savings from converting AC to reflective pavements in Boston

85

In addition to urban morphology, other contextual factors such as traffic loads, recycled contents as well as cleanliness of the electricity grid are also examined. The sensitivity analyses show that they do not affect the results significantly.

4.3.3 Effect on air temperature

Another known benefit of raising pavement albedo is its indirect effect on reducing the ambient air temperature. In this study, urban climate is simulated with Urban Weather Generator (UWG), where the monthly average air temperature change of increasing pavement albedo can be recorded.

Figure 4.7 shows the maximum air temperature reductions in Boston and Phoenix simulated from UWG for the ten different local climate zones (LCZs) specified in Stewart & Oke (2012) *(63)*. The effect of increasing pavement albedo on air temperature varies by LCZ, depending on the average building height, building density and building geometry. For Boston, the ambient temperature effect is more pronounced in low-density neighborhoods than in densely built areas. This is due to the fact that shadings of the buildings in dense neighborhoods offset some of the benefits from increasing pavement albedo. LCZ 9 exhibits the greatest air temperature reduction (0.25°C) among all LCZs. For Phoenix, however, the ambient temperature effect is more significant than it does to Boston due to lower building density overall.
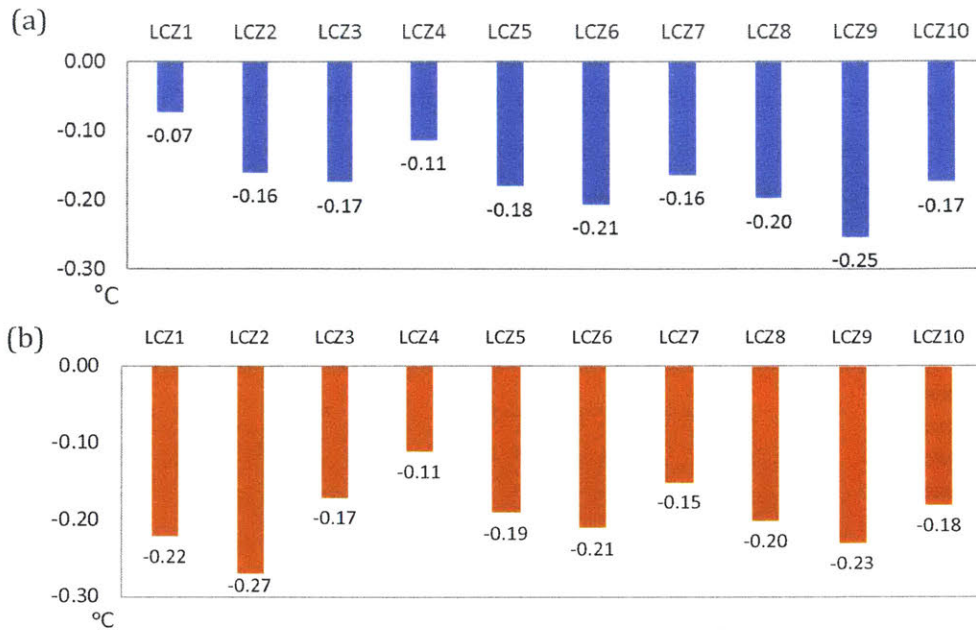
Figure 4.7 Maximum air temperature reductions for 10 LCZs due to 0.2 increase in pavement albedo in (a) Boston and (b) Phoenix

Seasonal average diurnal temperature changes for one of the 10 LCZs is shown in Figure 4.8. It can be seen that the air temperature reductions occur only during the daytime, while in the nighttime temperature increase as absorbed heat release from the surrounding buildings during the day. Of the four seasons, summertime (from June to August) experiences the highest reduction in daytime air temperature.
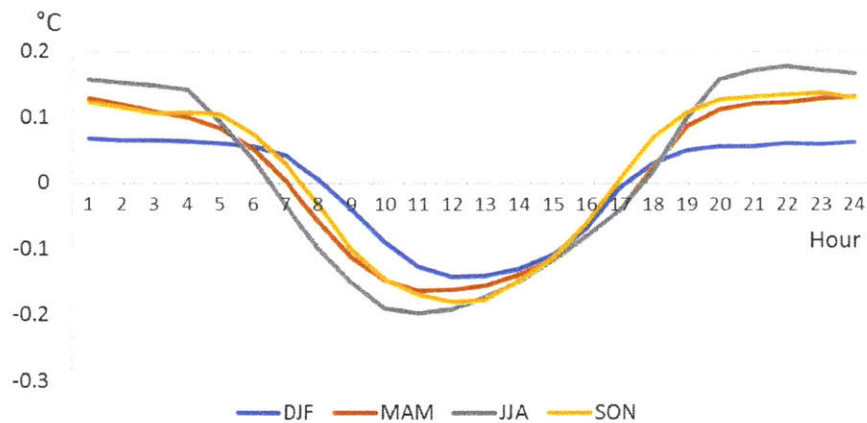
Figure 4.8 Seasonal average diurnal temperature changes for LCZ6 (open low-rise). DJF=Dec/Jan/Feb, MAM=Mar/Apr/May, JJA=Jun/Jul/Aug, SON=Sep/Oct/Nov

87

4.3.4 Uncertainty assessment

The analysis is conducted using a probabilistic approach, allowing for characterizing the probabilistic properties of the input data and output impact results. The breakdowns of total life cycle GWP impact and the use phase impact for Boston are presented in Figure 4.9 and Figure 4.10, respectively. It can be seen that the uncertainty with the life cycle impact is mainly driven by the use phase impact, which is primarily dominated by the roughness-induced PVI impact.
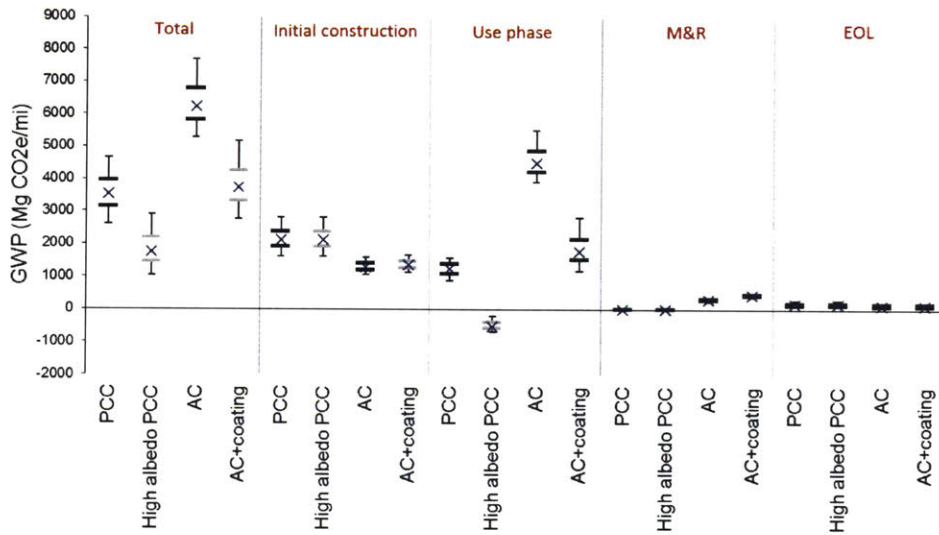
Figure 4.9 Breakdown of pavement life-cycle GWP impacts with uncertainties for conventional PCC and AC designs and reflective PCC and AC designs for Boston. Albedo impacts relative to baseline of average earth albedo (0.3)
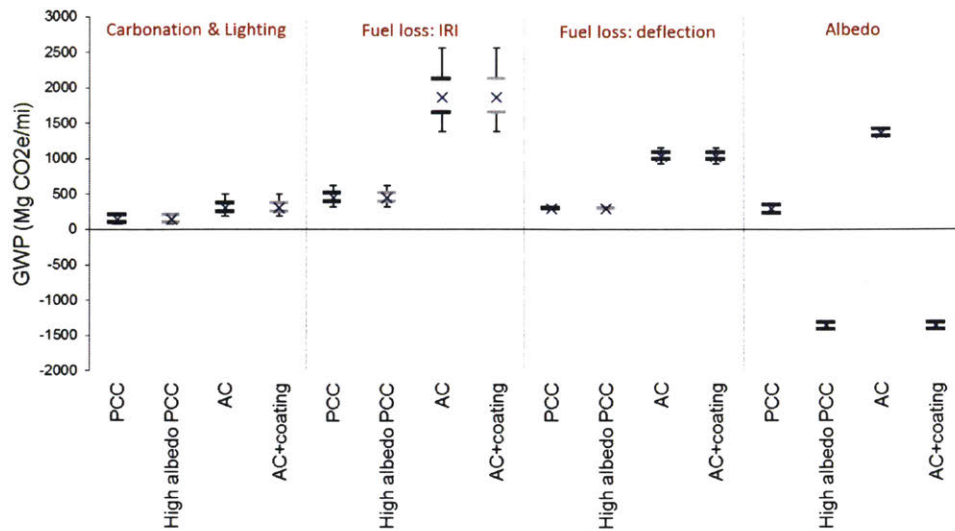
Figure 4.10 Breakdown of use phase GWP impacts with uncertainties for conventional PCC and AC designs and reflective PCC and AC designs for Boston. Albedo impacts relative to baseline of average earth albedo (0.3)

4.4 Conclusions

This study has implemented a pavement LCA model that accounts for all life cycle phases of a pavement (materials production, construction, use, maintenance, and end-of-life). Particularly, in the use phase, context-specific model is developed and applied for quantifying the impact of increasing pavement albedo. The probabilistic LCA model has been applied to a range of reflective pavement scenarios with different climate conditions. The results from the LCA help in understanding of the impact of pavement albedo on the overall GWP and how that varies by contexts. The following two research questions have been answered:

- What's the net impact of pavement albedo under different contexts?
- How do albedo impacts compare with other components in a pavement's life cycle?

Several conclusions can be drawn through an LCA case study of various reflective pavement strategies in Boston.

- For PCC designs, materials and construction is a big contributor to the total life cycle GWP impact. However, for AC designs, use phase impact drives the total

89

GWP. The relative magnitude of pavement albedo impact is comparable to that of the PVI impact in the use phase. Albedo can be a significant portion of pavement life cycle environmental impacts, but is context sensitive.

- The impact of increasing pavement albedo on BED depends greatly on urban morphology. In densely built neighborhoods, the burden from increased incident radiation is more significant than the reduced temperature effect. Therefore, reflective pavements is less favorable in dense neighborhoods than low density residential areas.

- RF is more significant in most neighborhoods, except in dense neighborhood where shadings from buildings block the solar radiation from getting to the canyon floor.

- Increasing pavement albedo has significant potential to mitigate impacts of climate change and UHI effects by offsetting GHG emissions and reducing urban canyon temperature. In the case of Boston, the 50-year GWP savings could be as much as 1,005 kton if all roads were converted to reflective pavements, equivalent to 1.25% of the total GHG emissions from the transportation sector in Boston, and a maximum air temperature reduction of 0.25°C can be expected in some neighborhoods.

CHAPTER 5 CONCLUDING REMARKS AND FUTURE WORK

Albedo, or surface reflectivity, is defined as the ratio of solar radiation reflected by a surface or an object, measured on a scale from zero (complete absorption) to one (complete reflection). Anthropogenic modifications to land surface due to urbanization have changed the surface albedo, which has direct and indirect impacts on local and global climate. On one hand, surface albedo changes can affect the amount of solar radiation going back to the space and alter the radiative balance at the top-of-atmosphere (TOA), exerting radiative forcing (RF). Indirectly, urban surfaces, due to their lower albedo and impervious properties, also contribute to a phenomenon known as "urban heat island" effect. The elevated temperature increases the demand for building cooling energy in order to maintain a comfort level, resulting in more greenhouse gas (GHG) emissions from generating the energy.

5.1 Conclusions

In this dissertation, two models for quantifying RF and BED impacts due to pavement albedo changes are presented.

Radiative forcing

To estimate the RF impact, we adapt an empirical analytical model from the literature and incorporate the effects of cloudiness and shadings in the urban area. The adapted

model we propose partially addresses the limitation of previous parameterized model by incorporating a cloudiness regression function to account for the effects of cloudiness and shadings in the urban area.

In the adapted model we develop, the effects of solar intensity, precipitable water, solar zenith angle and cloudiness on atmospheric transmittance are parameterized and calibrated using data from climate simulation. Data and model indicate that the transmittance factor has a positive correlation with solar intensity, and negative correlations with precipitable water, solar angle and cloudiness. Comparison of the results across the U.S. also reveals the spatial variation due to contextual variables.

A case study of the RF impact due to pavement albedo modifications in fourteen major U.S. cities is conducted, with location-specific data extracted from sophisticated climate simulations WRF. Ranges of the GWP savings are computed from two different models, the symmetric model and the adapted model, which reflect the uncertainties associated with the atmospheric transmittance, especially the cloudiness effect. For the case of Phoenix, the resulting mean f_a calculated from the simple symmetric model Eq. (2.6) is 0.617, and 0.729 from the parameterization model shown in Eq. (2.15). The discrepancy reveals different underlying assumptions regarding the downward and upward transmittance through the atmosphere. The symmetric model assumes symmetric processes and results in a smaller f_a (more is lost through the atmosphere than transmitted), while the parameterization is derived under clear-sky conditions so it will be an over-estimate as clouds are present some of the time everywhere. The adapted

model we propose, however, partially addresses the limitation of the parameterized model by incorporating a cloudiness regression function $g(cloud)$. The f_a value calculated with this model is 0.683, which is greater than the f_a estimated from simple symmetric model, and smaller than the clear-sky f_a calculated using Eq. (2.7).

The method proposed here is a more accurate estimate of the f_a value and thus the associated GWP. Comparison of the results across the U.S. also reveals the spatial variation due to contextual variables.

Building energy demand

For BED, several existing simulation tools are combined to account for the interactions between buildings and surrounding environment. Experimental design is carried out to better understand the influence of urban morphology on BED due to pavement albedo changes. The trade-off between two mechanisms: incident radiation and ambient temperature is investigated and discussed based on simulation results.

Which mechanism is dominant depends on a number of contextual factors. Overall, the hypothesis that urban morphology and pavement albedo have significant impacts on BED is confirmed. Several morphological parameters are identified as the most influential factors. Among those parameters, canyon aspect ratio and building density are found to have greater influence on the amount of incident radiation receiving by building surfaces, correlating with the solar heat gains of building thus the BED. The surface-to-volume ratio also correlates well with BED, but shows a greater ambient

temperature effect than that of direct incident radiation. Results from the experimental design and the case study of Boston and Phoenix validate our hypothesis that the impact of pavement albedo change on BED is context dependent. Increasing pavement albedo usually create burdens on BED for densely-built neighborhoods while low-density neighborhoods are more likely to benefit from more reflective pavements.

A case study of pavement LCA incorporating the RF and BED impacts due to pavement albedo modifications in two urban area is conducted, with location-specific data extracted from climate simulations and GIS datasets. Increasing pavement albedo has significant potential to mitigate impacts of climate change and UHI effects by offsetting GHG emissions and reducing urban canyon temperature. In the case of Boston, the 50-year GWP savings could be as much as 1,005 kton if all roads were converted to reflective pavements, equivalent to 1.25% of the total GHG emissions from the transportation sector in Boston, and a maximum air temperature reduction of 0.25°C can be expected in some neighborhoods.

This study is the first attempt to compare RF and BED impacts due to pavement albedo modifications under the same context, and it is a first estimate of the net benefit of reflective pavements at an urban scale while most studies in the literature only quantify the impact of RF or BED individually. Comparison of the results across the different LCZs reveals the importance of developing context-specific models for albedo impact estimation. Urban-scale impact quantification is also necessary as albedo modifications can have different and even contradicting impact on BED depending on urban

morphology. Comprehensive assessment taking into account both RF and BED is recommended when evaluating reflective pavements as a global warming mitigation strategy.

5.2 Limitations and Future Work

The approach and context-specific models developed in this study requires location-specific data about the specific neighborhood of interest, which can be obtained freely online upon request. The models are ready for implementation and integration into in pavement LCA. There are, however, some limitations with the analytical model as well as the simulation tools within the BED models, which limit their capabilities of dealing with complex geometries, large areas and/or multiple zones.

Radiative forcing

The analytical model for RF impact takes advantage of simulated data to derive statistical relationships among atmospheric transmittance and other contextual factors. The model implicitly accounts for the effect of multiple scattering and absorption of radiation globally within the atmosphere. Local impact of changing albedo can be calculated if location-specific incident shortwave solar radiation and other contextual parameters can be used instead of global average value. It provides an easy way to approximate the direct impacts of changing surface albedo in terms of radiative forcing and global warming potential, which can be easily applied to any geographic area.

There are, however, challenges and limitations that could be improved in further research. First of all, location-specific data on T_a or f_a are not readily available. While incident shortwave solar radiation at TOA (R_{TOA}) and at the surface (R_s) can be obtained from historical satellite measurements or climate simulations, atmospheric transmittance factor T_a and f_a are not typical parameters tracked by satellite observations. Second, the effect of aerosols has not been evaluated in this model due to the lack of data. For locations known for air pollution such as Los Angeles, the model needs to be re-evaluated with aerosol data. Third, data on the evolution of surface albedo, particularly pavement albedo, is not available currently. Surface albedo varies from year to year. As pavement ages, concrete surface tends to get darker so the albedo gets smaller, while asphalt surface gradually gets brighter so the albedo of asphalt becomes greater. Pavement albedo could also vary seasonally due to snow, rain and even the traffic on the pavement. Long-term measurements of albedo have been undertaken by some other researchers in order to better characterize the changes of albedo ($\Delta\alpha_s$). In addition, the analytical model described above uses an average value of 0.4 for the effect of shadings. The urban transmittance factor τ can also be context-dependent, as it can be affected by the urban geometry such as building height and density, vegetation, etc. Further simulation is required to validate the urban canyon transmittance under different conditions. Furthermore, the analytical model described in Chapter 2 is limited to calculating the shortwave radiative forcing effect, as changing surface albedo has been considered to be a shortwave radiative forcing agent; it affects the radiative balance primarily through shortwave radiation. However, it would be more defensible if

longwave radiative forcing effect could also be quantified, even if it is supposed to be negligible compared to shortwave radiative forcing.

Building energy demand

There is inherent uncertainty within the numerical simulations due to the chaotic nature of the open environment and the complexity of the energy system. In order to achieve first-order relationship and reduce computational cost, we assume one thermal zone per time in building energy modeling. Thus, each thermal zone needs to be analyzed independently, and the interaction of different zones within a building cannot be assessed.

The UWG is capable of capturing the radiative and heat fluxes from the pavement surface and the adjacent buildings, but the representation of urban canyon in the UWG is simplified to reduce computational cost. There are also some assumptions that we made about the urban morphology and building geometry when conducting the experimental design. Realistic urban neighborhoods should be treated specifically with extra details in order to gain better insights regarding the effectiveness of increasing pavement albedo as a global warming and UHI mitigation strategy. UWG assumes a simple homogenous urban canyon morphology and employs a heat balance method to simulate canyon temperature. Variation and dynamics in temperature cannot be resolved, which may introduce uncertainty in evaluating the cooling effect of reflective pavements.

Finally, a more comprehensive analysis of urban neighborhoods with various morphologies will be needed to the get a better understanding of the relative value of higher albedo pavements in different contexts. The authors will also extend the analysis to a wider ranges of cities with or without GIS datasets. In addition, the effects of building properties on BED should also be evaluated. The outcomes of this study will help urban planners or decision makers make informed decisions on whether pavement albedo enhancement is an option worth pursuing in any given urban area/neighborhood.

REFERENCE

1. Santero, N., Masanet, E. and Horvath, A. Life Cycle Assessment of Pavements : A Critical Review of Existing Literature and Research. , 2010.

2. Akbarian, M., Moeini-Ardakani, S. S., Ulm, F.-J. and Nazzal, M. Mechanistic Approach to Pavement-Vehicle Interaction and Its Impact on Life-Cycle Assessment. *Transportation Research Record: Journal of the Transportation Research Board*, Vol.2306, 2012. pp.171–179.

3. Levinson, R. Life-Cycle Assessment and Co-Benefits of Cool Pavements. Vol., 2012. pp.1–2.

4. Rosenfeld, A. H., Akbari, H., Romm, J. J. and Pomerantz, M. Cool Communities: Strategies for Heat Island Mitigation and Smog Reduction. *Energy and Buildings*, Vol.28(1), 1998. pp.51–62.

5. Akbari, H., Menon, S. and Rosenfeld, A. Global Cooling: Increasing World-Wide Urban Albedos to Offset CO2. *Climatic Change*, Vol.94, 2009. pp.275–286.

6. Santero, N., Loijos, A. and Ochsendorf, J. Greenhouse Gas Emissions Reduction Opportunities for Concrete Pavements. *Journal of Industrial Ecology*, Vol.17(6), 2013. pp.859–868.

7. Santero, N. and Horvath, A. Supplemental Information. Global Warming Potential of Pavements. *Environmental Research Letters*, Vol.4(3), 2009. p.34011.

8. Rose, L. S., Akbari, H. and Taha, H. Characterizing the fabric of the urban environment: A case study of Greater Houston, Texas. Lawrence Berkeley National Laboratory, , 2003.

9. Ramaswamy, V. Radiative forcing of climate change. In: Houghton JT et al (eds) Climate change 2001: the scientific basis. Contribution of working group I to the third assessment report of the intergovernmental panel on climate change. Cambridge University Press, Cambridge. pp. 349–416. , 2001.

10. Myhre, G., Shindell, D., Bréon, F.-M., *et al.* Anthropogenic and Natural Radiative Forcing. In: Climate Change 2013: The Physical Science Basis. Contribution of Working Group I to the Fifth Assessment Report of the Intergovernmental Panel on Climate Change. Cambridge University Press, Cambridge, United Kingdom and New York, NY, USA. , 2013.

11. Menon, S., Akbari, H., Mahanama, S., Sednev, I. and Levinson, R. Radiative Forcing and Temperature Response to Changes in Urban Albedos and

Associated CO2 Offsets. *Environmental Research Letters*, Vol.5(1), 2010. p.14005.

12. Akbari H, Davis, S., Dorsano, S., Huang, J. and Winnett, S. Cooling our communities: a guidebook on tree planting and light-colored surfacing. U.S. Department of the Interior, Environmental Protection Agency, Washington, DC. , 1992.

13. Akbari, H., Konopacki, S. and Pomerantz, M. Cooling Energy Savings Potential of Reflective Roofs for Residential and Commercial Buildings in the United States. *Energy*, Vol.24(5), 1999. pp.391–407.

14. Levinson, R. and Akbari, H. Potential Benefits of Cool Roofs on Commercial Buildings: Conserving Energy, Saving Money, and Reducing Emission of Greenhouse Gases and Air Pollutants. *Energy Efficiency*, Vol.3(1), 2009. pp.53–109.

15. Akbari, H. and Konopacki, S. Calculating Energy-Saving Potentials of Heat-Island Reduction Strategies. *Energy Policy*, Vol.33(6), 2005. pp.721–756.

16. Yaghoobian, N., Kleissl, J. and Krayenhoff, E. S. Modeling the Thermal Effects of Artificial Turf on the Urban Environment. *Journal of Applied Meteorology and Climatology*, Vol.49(3), 2010. pp.332–345.

17. Yaghoobian, N. and Kleissl, J. Effect of Reflective Pavements on Building Energy Use. *Urban Climate*, Vol.2, 2012. pp.25–42.

18. Lenton, T. M. and Vaughan, N. E. The Radiative Forcing Potential of Different Climate Geoengineering Options. *Atmospheric Chemistry and Physics*, Vol.9(15), 2009. pp.5539–5561.

19. Muñoz, I., Campra, P. and Fernández-Alba, A. R. Including CO2-Emission Equivalence of Changes in Land Surface Albedo in Life Cycle Assessment. Methodology and Case Study on Greenhouse Agriculture. *The International Journal of Life Cycle Assessment*, Vol.15(7), 2010. pp.672–681.

20. Bright, R. M., Cherubini, F. and Strømman, A. H. Climate Impacts of Bioenergy: Inclusion of Carbon Cycle and Albedo Dynamics in Life Cycle Impact Assessment. *Environmental Impact Assessment Review*, Vol.37, 2012. pp.2–11.

21. Yaghoobian, N. and Kleissl, J. Effect of Reflective Pavements on Building Energy Use. *Urban Climate*, Vol.2, 2012. pp.25–42.

22. Synnefa, A., Santamouris, M. and Akbari, H. Estimating the Effect of Using Cool Coatings on Energy Loads and Thermal Comfort in Residential Buildings in Various Climatic Conditions. *Energy and Buildings*, Vol.39(11), 2007.

pp.1167–1174.

23. Betts, R. a. Offset of the Potential Carbon Sink from Boreal Forestation by Decreases in Surface Albedo. *Nature*, Vol.408(6809), 2000. pp.187–190.

24. López-Saldaña, G., Bistinas, I. and Pereira, J. M. C. Global Analysis of Radiative Forcing from Fire-Induced Shortwave Albedo Change. *Biogeosciences Discussions*, Vol.11(5), 2014. pp.7775–7796.

25. Cherubini, F., Bright, R. M. and Strømman, A. H. Site-Specific Global Warming Potentials of Biogenic CO_2 for Bioenergy: Contributions from Carbon Fluxes and Albedo Dynamics. *Environmental Research Letters*, Vol.7(4), 2012. p.45902.

26. IPCC. Climate Change 2007: The Physical Science Basis, Summary for Policymakers, Intergovernmental Panel on Climate Change. Intergovernmental Panel on Climate Change (IPCC), Geneva, Switzerland. , 2007.

27. Lenton, T. M. and Vaughan, N. E. The Radiative Forcing Potential of Different Climate Geoengineering Options. *Atmospheric Chemistry and Physics Discussions*, Vol.9(1), 2009. pp.2559–2608.

28. NASA. NASA Atmospheric Science Data Center: Surface Meteorology and Solar Energy (Release 6.0). , 2015. at <https://eosweb.larc.nasa.gov/cgi-bin/sse/sse.cgi?>

29. Lacis, A. A. and Hansen, J. A Parameterization for the Absorption of Solar Radiation in the Earth's Atmosphere. *Journal of the Atmospheric Sciences*, Vol.31(1), 1974. pp.118–133.

30. Chen, T. S. and Ohring, G. Clear-Sky Planetary and Surface Albedos: A Parameterization for Simple Models. Vol.5(6), 1985. pp.141–144.

31. Li, Z. and Garand, L. Estimation of Surface Albedo from Space: A Parameterization for Global Application. *Journal of Geophysical Research*, Vol.99(D4), 1994. p.8335.

32. Anslow, F. S., Hostetler, S., Bidlake, W. R. and Clark, P. U. Distributed Energy Balance Modeling of South Cascade Glacier, Washington and Assessment of Model Uncertainty. *Journal of Geophysical Research*, Vol.113(F2), 2008. p.F02019.

33. (Lisette) Klok, E. J. and Oerlemans, J. Model Study of the Spatial Distribution of the Energy and Mass Balance of Morteratschgletscher, Switzerland. *Journal of Glaciology*, Vol.48(163), 2002. pp.505–518.

34. Mölg, T., Cullen, N. J. and Kaser, G. Solar Radiation, Cloudiness and

Longwave Radiation over Low-Latitude Glaciers: Implications for Mass-Balance Modelling. *Journal of Glaciology*, Vol.55(190), 2009. pp.292–302.

35.   Foyo-Moreno, I., Alados, I., Olmo, F. J., Vida, J. and Alados-Arboledas, L. On the Use of a Cloud Modification Factor for Solar UV (290±385 Nm) Spectral Range.

36.   Fitzpatrick, M. F., Brandt, R. E., Warren, S. G., *et al.* Transmission of Solar Radiation by Clouds over Snow and Ice Surfaces: A Parameterization in Terms of Optical Depth, Solar Zenith Angle, and Surface Albedo. *http://dx.doi.org/10.1175/1520-0442(2004)017<0266:TOSRBC>2.0.CO;2*, Vol., 2004. p.

37.   Pellicciotti, F., Raschle, T., Huerlimann, T., Carenzo, M. and Burlando, P. Transmission of Solar Radiation through Clouds on Melting Glaciers: A Comparison of Parameterizations and Their Impact on Melt Modelling. *Journal of Glaciology*, Vol.57(202), 2011. pp.367–381.

38.   Bueno, B., Norford, L., Hidalgo, J. and Pigeon, G. The Urban Weather Generator. *Journal of Building Performance Simulation*, Vol.(February 2015), 2012. pp.1–13.

39.   FHWA. Clear Zone and Horizontal Clearance - Geometric Design - Design - Federal Highway Administration. at <https://www.fhwa.dot.gov/programadmin/clearzone.cfm>

40.   Briggs, R. S., Lucas, R. G. and Taylor, Z. T. Climate Classification for Building Energy Codes and Standards. Vol., 2002. p.

41.   Energy – UN-Habitat. at <https://unhabitat.org/urban-themes/energy/>

42.   Magyari, Á., Veronika Vizi, K., Reith, A. and Szabó DLA, Á. City-scale energy modeling - Comparative review of city-scale energy modelling approaches. , 2016.

43.   Pravin Bhiwapurkar. Urban Microclimates and Energy Efficient Buildings. in *Special Issue: Future of Architectural Research/ARCC 2015 Conference*, , 2015.

44.   Xiao, Y. Urban morphology and housing market. Springer, , 2017.

45.   Rode, P., Keim, C., Robazza, G., Viejo, P. and Schofield, J. Cities and Energy: Urban Morphology and Residential Heat-Energy Demand. *Environment and Planning B: Planning and Design*, Vol.41(1), 2014. pp.138–162.

46.   Zakhour, S. Urban Morphology and Microclimate Response – Overview and Case Study. *QScience Proceedings*, Vol.2016p.

47. Morganti, M., Coch Roura, H. and Cecere, C. The Effects of Urban Obstructions in Mediterranean Climates: Built Form Typology, Density and Energy. *ACE: Architecture, City and Environment*, Vol.7(19), 2012. pp.13–26.

48. Morganti, M., Salvati, A., Coch, H. and Cecere, C. Urban Morphology Indicators for Solar Energy Analysis. *Energy Procedia*, Vol.134, 2017. pp.807–814.

49. Salat, S. Energy Loads, CO_2 Emissions and Building Stocks: Morphologies, Typologies, Energy Systems and Behaviour. *Building Research & Information*, Vol.37(5–6), 2009. pp.598–609.

50. Zhang, J., Heng, C. K., Malone-Lee, L. C., *et al*. Evaluating Environmental Implications of Density: A Comparative Case Study on the Relationship between Density, Urban Block Typology and Sky Exposure. *Automation in Construction*, Vol.22, 2012. pp.90–101.

51. Pisello, A. L., Castaldo, V. L., Poli, T. and Cotana, F. Simulating the Thermal-Energy Performance of Buildings at the Urban Scale: Evaluation of Inter-Building Effects in Different Urban Configurations. *Journal of Urban Technology*, Vol.21(1), 2014. pp.3–20.

52. Salvati, A., Coch, H. and CECERE, C. Urban Morphology and Energy Performance: The Direct and Indirect Contribution in Mediterranean Climate. in *PLEA2015 Architecture in (R)Evolution*, , 2015.

53. Han, Y., Taylor, J. E. and Pisello, A. L. Exploring Mutual Shading and Mutual Reflection Inter-Building Effects on Building Energy Performance. *Applied Energy*, Vol.185, 2017. pp.1556–1564.

54. Monaghan, A. J., Hu, L., Brunsell, N. A., Barlage, M. and Wilhelmi, O. V. Evaluating the Impact of Urban Morphology Configurations on the Accuracy of Urban Canopy Model Temperature Simulations with MODIS. *Journal of Geophysical Research: Atmospheres*, Vol.119(11), 2014. pp.6376–6392.

55. Kikegawa, Y., Genchi, Y., Yoshikado, H. and Kondo, H. Development of a Numerical Simulation System toward Comprehensive Assessments of Urban Warming Countermeasures Including Their Impacts upon the Urban Buildings' Energy-Demands. *Applied Energy*, Vol.76(4), 2003. pp.449–466.

56. Kikegawa, Y., Genchi, Y., Kondo, H. and Hanaki, K. Impacts of City-Block-Scale Countermeasures against Urban Heat-Island Phenomena upon a Building's Energy-Consumption for Air-Conditioning. *Applied Energy*, Vol.83(6), 2006. pp.649–668.

57. Salamanca, F., Krpo, A., Martilli, A. and Clappier, A. A New Building Energy Model Coupled with an Urban Canopy Parameterization for Urban Climate

Simulations—part I. Formulation, Verification, and Sensitivity Analysis of the Model. *Theoretical and Applied Climatology*, Vol.99(3–4), 2010. pp.331–344.

58.   Krpo, A., Salamanca, F., Martilli, A. and Clappier, A. On the Impact of Anthropogenic Heat Fluxes on the Urban Boundary Layer: A Two-Dimensional Numerical Study. *Boundary-Layer Meteorology*, Vol.136(1), 2010. pp.105–127.

59.   Salamanca, F., Martilli, A., Tewari, M., *et al.* A Study of the Urban Boundary Layer Using Different Urban Parameterizations and High-Resolution Urban Canopy Parameters with WRF. *Journal of Applied Meteorology and Climatology*, Vol.50(5), 2011. pp.1107–1128.

60.   Mauree, D., Coccolo, S., Kaempf, J. and Scartezzini, J.-L. Multi-Scale Modelling to Evaluate Building Energy Consumption at the Neighbourhood Scale. *PLOS ONE*, Vol.12(9), 2017. p.e0183437.

61.   Quan, S. J., Economou, A., Grasl, T. and Yang, P. P.-J. Computing Energy Performance of Building Density, Shape and Typology in Urban Context. *Energy Procedia*, Vol.61, 2014. pp.1602–1605.

62.   Grasshopper - Algorithmic Modeling for Rhino. at <http://www.grasshopper3d.com/>

63.   Stewart, I. D., Oke, T. R., Stewart, I. D. and Oke, T. R. Local Climate Zones for Urban Temperature Studies. *Bulletin of the American Meteorological Society*, Vol.93(12), 2012. pp.1879–1900.

64.   Ladybug Tools. at <http://www.food4rhino.com/app/ladybug-tools>

65.   Rhinoceros. at <https://www.rhino3d.com/>

66.   Martins, T. and Sc, D. DOE Sensitivity Analysis of Urban Morphology Factors Regarding Solar Irradiation on Buildings Envelope in the Brazilian Tropical Context. Vol.(December), 2014. pp.1–8.

67.   U.S. Department of Energy (DOE). EnergyPlus Version 8.8.0 Documentation: Engineering Reference. , 2017. at <https://energyplus.net/documentation>

68.   Nakano, A., Bueno, B., Norford, L. and Reinhart, C. F. URBAN WEATHER GENERATOR – A NOVEL WORKFLOW FOR INTEGRATING URBAN HEAT ISLAND EFFECT WITHIN URBAN DESIGN PROCESS.

69.   Bueno, B., Norford, L., Hidalgo, J. and Pigeon, G. The Urban Weather Generator. *Journal of Building Performance Simulation*, Vol.6(February 2015), 2012. pp.1–13.

70. Bueno, B., Roth, M., Norford, L. and Li, R. Computationally Efficient Prediction of Canopy Level Urban Air Temperature at the Neighbourhood Scale. *Urban Climate*, Vol.9, 2014. pp.35–53.

71. MassGIS (Bureau of Geographic Information) | Mass.gov. at <https://www.mass.gov/orgs/massgis-bureau-of-geographic-information>

72. ASU Library Map and Geospatial Hub. at <https://lib.asu.edu/geo>

73. US Census Bureau. TIGER/Line® Shapefiles and TIGER/Line® Files. at <https://www.census.gov/geo/maps-data/data/tiger-line.html>

74. DOE Building Energy Codes Program. ANSI/ASHRAE/IES Standard 90.1-2010 | Building Energy Codes Program. , 2011. at <https://www.energycodes.gov/training-courses/ansiashraeies-standard-901-2010>

75. Behsh, B. BUILDING FORM AS AN OPTION FOR ENHANCING THE INDOOR THERMAL CONDITIONS. *Session*, Vol.18p.

76. U.S. Environmental Protection Agency. Emissions & Generation Resource Integrated Database (eGRID). , 2016. at <https://www.epa.gov/energy/emissions-generation-resource-integrated-database-egrid>

77. US EPA. Greenhouse Gases Equivalencies Calculator - Calculations and References. , 2017. at <https://www.epa.gov/energy/greenhouse-gases-equivalencies-calculator-calculations-and-references>

78. Santero, N. and Horvath, A. Global Warming Potential of Pavements. *Environmental Research Letters*, Vol.4(3), 2009. p.34011.

79. Harvey, J., Kendall, A., Santero, N., *et al*. Pavement Life Cycle Assessment Workshop, May 5–7, 2010 in Davis, California, USA. *The International Journal of Life Cycle Assessment*, Vol.16(9), 2011. pp.944–946.

80. Wang, T., Lee, I.-S., Kendall, A., *et al*. Life Cycle Energy Consumption and GHG Emission from Pavement Rehabilitation with Different Rolling Resistance. *Journal of Cleaner Production*, Vol.33, 2012. pp.86–96.

81. Gilbert, H. E., Rosado, P. J., Ban-Weiss, G., *et al*. Energy and Environmental Consequences of a Cool Pavement Campaign. *Energy and Buildings*, Vol., 2017. p.

82. Akbari, H., Shea Rose, L. and Taha, H. Analyzing the Land Cover of an Urban Environment Using High-Resolution Orthophotos. *Landscape and Urban Planning*, Vol.63(1), 2003. pp.1–14.

83. Pomerantz, M., Akbari, H., Chen, A., Taha, H. and Rosenfeld, A. H. Paving materials for heat island mitigation. , 1997.

84. US EPA. Reducing Urban Heat Islands: Compendium of Strategies I Heat Island Effect I US EPA. *US EPA*, Vol., 2013. p.

85. Santamouris, M. Cooling the Cities - A Review of Reflective and Green Roof Mitigation Technologies to Fight Heat Island and Improve Comfort in Urban Environments. *Solar Energy*, Vol.103, 2014. pp.682–703.

86. Pomerantz, M., Rosado, P. J. and Levinson, R. A Simple Tool for Estimating City-Wide Annual Electrical Energy Savings from Cooler Surfaces. *Urban Climate*, Vol.14, 2015. pp.315–325.

87. Noshadravan, A., Wildnauer, M., Gregory, J. and Kirchain, R. Comparative Pavement Life Cycle Assessment with Parameter Uncertainty. *Transportation Research Part D: Transport and Environment*, Vol.25, 2013. pp.131–138.

88. Xu, X., Noshadravan, A., Gregory, J. and Kirchain, R. Scenario Analysis of Comparative Pavement Life Cycle Assessment. *International Symposium on Pavement LCA 2014*, Vol., 2014. pp.13–26.

89. American Association of State Highway and Transportation Officials (AASHTO). Mechanistic-empirical Pavement Design Guide: A Manual of Practice. AASHTO, , 2008.

90. National Cooperative Highway Research Program (NCHRP). Guide for Mechanistic-Empirical Pavement Design of New and Rehabilitated Pavement Structure. *NCHRP Report 1-37A*, , 2004.

91. Zaabar, I. and Chatti, K. Calibration of HDM-4 Models for Estimating the Effect of Pavement Roughness on Fuel Consumption for U. S. Conditions. *Transportation Research Record: Journal of the Transportation Research Board*, Vol.2155, 2010. pp.105–116.

92. Weidema, B. P., Bauer, C., Hischier, R., *et al.* Overview and Methodology, Data Quality Guideline for the Ecoinvent Database Version 3. *Ecoinvent Report 1(v3)*, St. Gallen: The ecoinvent Centre, , 2013.

93. ACPA. Albedo: A Measure of Pavement Surface Reflectance. American Concrete Pavement Association, Skokie, IL. , 2002.

94. Levinson, R. Life-Cycle Assessment and Co-Benefits of Cool Pavements. , 2017. at <https://www.arb.ca.gov/research/single-project.php?row_id=65149>

95. City of Boston. City of boston greenhouse gas emissions inventory 2005-2015. , 2018.

96. The Intergovernmental Panel on Climate Change (IPCC). Good Practice Guidance and Uncertainty Management in National Greenhouse Gas Inventories. , 2000.

APPENDIX A

Table A1. Parameters for the energy simulation for the building prototype in 5A climate zone complying with the ASHRAE standards 90.1-2010

Parameter	
Roof U (W/m²K)	0.358
Wall U (W/m²K)	0.698
Window U (W/m²K)	3.241
Window SHGC	0.385
Heating COP	0.78
Cooling COP	3.167
Window-to-wall ratio (WWR)	0.3
Occupancy Factor	0.732
Illumination Factor	1
Mechanical Ventilation Supply Ratio (liter/s/m²)	0.125
Occupancy (m²/person)	17.696
Lighting (W/m²)	11.84
Roof solar Absorbance	0.7
Wall solar Absorbance	0.92
Emissivity of roof	0.9
Emissivity of wall	0.9
Primary Source for Heating (1 elect; 2 gas)	2
Primary Source for Cooling (1 elect; 2 gas)	1
Floor Height	4
Infiltration ACH	0.011

APPENDIX B

Table B1. Life Cycle Assessment (LCA) Inputs Data Sources and Assumptions

Lifecycle Phase		Quantity Data Source	COV[1]	Impact Data Source	Key Assumptions
Materials					
	Steel reinforcement	MEPDG	0.073	Worldsteel	70% recycled content; 70% recycled at EOL
Concrete		MEPDG	0.058	n/a	Mix design from MEPDG
	Cement	MEPDG	0.060	*See Table B2*	See Cement LCA inputs
	Cement Materials	PCA Environmental Surveys	-	*See Table B2*	See Cement LCA inputs
	Water	MEPDG	0.107	Ecoinvent	
	Fly ash		0.460	PE International	
	Aggregate	MEPDG	0.063	Ecoinvent	
	Concrete Mixing	NCSA/Zapata	0.302	Ecoinvent	Diesel
Asphalt Concrete		MEPDG	0.058	n/a	
	Bitumen	MEPDG	0.060	Ecoinvent	Bitumen, at refinery/RER
	Aggregate	MEPDG	0.063	Ecoinvent	
Cement Stabilized SG		MEPDG	0.058	n/a	
	Cement	Ohio DOT	0.072	*See Table B2*	See Cement LCA inputs
	Soil	Ohio DOT	0.070	n/a	
Cement Treated Agg Base		MEPDG	0.058	n/a	
	Cement	Ohio DOT	0.072	*See Table B2*	See Cement LCA inputs
	Aggregate	Ohio DOT	0.075	Ecoinvent	
PATB		MEPDG	0.058	n/a	
	Bitumen	FL DOT	0.072	Ecoinvent	
	Aggregate	FL DOT	0.075	Ecoinvent	
Construction					

---

[1] COV = standard deviation/mean; calculated from pedigree matrix (underlying normal distribution)

Lifecycle Phase		Quantity Data Source	COV[1]	Impact Data Source	Key Assumptions
	Concrete Paving	Chappat and Bilal (2003)/IVL	0.215	Ecoinvent	Diesel
	Asphalt Paving	Chappat and Bilal (2003)/IVL	0.215	Ecoinvent	Diesel
	Placement of other layers	Chappat and Bilal (2003)/IVL	0.229	Ecoinvent	Diesel

Transportation			Avg (km)	SD (km)[2]		
Concrete (km)	Truck	U.S. Commodity Flow Survey (2007)	40.2	8.4	Ecoinvent	Concrete truck (tank)
Steel (km)	Truck	BTS (2007) – Articles of Base Metal	684	143	Ecoinvent	
	Rail	BTS (2007) – Articles of Base Metal	1624	155.1	Ecoinvent	
Cement (km)	Truck	PCA Environmental Surveys	201	48.2	Ecoinvent	
	Rail	PCA Environmental Surveys	430	68.5	Ecoinvent	
	Water	PCA Environmental Surveys	644	644	Ecoinvent	
Fly Ash	Truck	BTS (2007) – Waste and scrap	201	42.1	Ecoinvent	
	Rail	BTS (2007) – Waste and scrap	589	56.3	Ecoinvent	
	Water	BTS (2007) – Waste and scrap	1880	75.3	Ecoinvent	
Aggregates	Truck	BTS (2007) – Gravel and crushed stone	88.5	18.5	Ecoinvent	
	Rail	BTS (2007) – Gravel and crushed stone	684	65.3	Ecoinvent	
	Water	BTS (2007) – Gravel and crushed stone	620	24.8	Ecoinvent	

---

[2] Standard deviation for transportation calculated from empirical data (arithmetic std dev) and pedigree matrix (underlying normal)

Lifecycle Phase		Quantity Data Source	COV[1]	Impact Data Source		Key Assumptions
Bitumen	Truck	BTS (2007) – Coal and petroleum products	158	33.0	Ecoinvent	
	Rail	BTS (2007) – Coal and petroleum products	1893	181	Ecoinvent	
	Water	BTS (2007) – Coal and petroleum products	1207	48.3	Ecoinvent	
Waste	Truck	assumption	50	10.5	Ecoinvent	
Use						
	Carbonation	Lagerblad (2005)	0.104	Lagerblad (2005)		
	Lighting	Electricity	Santero (2009)	0.045	Ecoinvent (electricity)	US average grid mix
		Tech Efficacy	Mn/DOT Roadway Lighting	0.073	n/a	
	Albedo	Radiative Forcing	Akbari et al (2009)	0.110	Akbari et al (2009)	38 kg CO_2e/m^2/0.15 decrease in albedo
		Urban Heat Island Effect	Rosenfeld et al (1998)	0.228	Rosenfeld et al (1998)	4.85×10^{-3} kg CO_2e/m^2/0.01 decrease in albedo
	PVI	Roughness	MEPDG	0.058	n/a	
		Average Fuel Use	FHWA Statistics	0.039	n/a	Car: 23.7 mpg Truck: 6.5 mpg
		AADT	FHWA Statistics	0.038	n/a	
		AADTT	FHWA Statistics	0.038	n/a	
		AADT % increase	FHWA Statistics	0.100	n/a	
		AADTT % increase	MEPDG	0.058	n/a	
		Fuel increase due to roughness	Zaabar and Chatti (2010)	0.361	n/a	Same source for cars and trucks

Lifecycle Phase			Quantity Data Source	COV[1]	Impact Data Source	Key Assumptions
		Gas	(based on purely mathematical formula using above inputs)	0.017	Ecoinvent: (divided by amount of fuel used) (Operation, passenger car, petrol, fleet average 2010/RER U)	Gas: 6.073 lb/gal
		Diesel	(based on purely mathematical formula using above inputs)	0.017	Ecoinvent: (divided by amount of fuel used) (Operation, lorry >16t, fleet average/RER U)	Diesel: 6.943 lb/gal
	PVI	Deflection				
		Gas	(from Mehdi)	0.365	Ecoinvent: (divided by amount of fuel used) (Operation, passenger car, petrol, fleet average 2010/RER U)	Gas: 6.073 lb/gal
		Diesel	(from Mehdi)	0.365	Ecoinvent: (divided by amount of fuel used) (Operation, lorry >16t, fleet average/RER U)	Diesel: 6.943 lb/gal
Maintenance						
	Onsite activities: diamond grinding, joint sawing, milling, overlay placement		International Grooving & Grinding Association (IGGA) (2009)	0.501	Ecoinvent	Diesel
	Traffic Delay					
		Fuel loss	Santero (2009)	0.459	n/a	
		User cost	RealCost	0.039	n/a	
		Work Zone Speed		0.459	n/a	
		Gas	(based on purely mathematical formula using above inputs)	0.017	Ecoinvent: (divided by amount of fuel used) (Operation, passenger car, petrol, fleet average 2010/RER U)	Gas: 6.073 lb/gal

Lifecycle Phase		Quantity Data Source	COV[1]	Impact Data Source	Key Assumptions
	Diesel	(based on purely mathematical formula using above inputs)	0.017	Ecoinvent: (divided by amount of fuel used) (Operation, lorry >16t, fleet average/RER U)	Diesel: 6.943 lb/gal
	Landfilling		0.127	Ecoinvent	Half of all recovered waste is landfilled
	Crushing/recycling concrete	Stripple 2001	0.327	Ecoinvent	Energy required to crush aggregate
	Excavation	IVL (2001)	0.340	Ecoinvent	

Table B2. Cement LCA Inputs and Assumptions

Cement LCA Inputs	Impact Data (Base Case) Source	Key Assumptions
Energy		
Gasoline	USLCI – Gasoline combusted in equipment/US	Impact Uncertainty: Ecoinvent – Heat production, light fuel oil, at industrial furnace 1MW/RER
Middle Distillates	USLCI – Diesel, combusted in industrial boiler/US	Impact Uncertainty: Ecoinvent – Heat production, light fuel oil, at industrial furnace 1MW/RER
Coal	USLCI – Bituminous coal, combusted in industrial boiler/US	Impact Uncertainty: Ecoinvent – Heat, at hard coal industrial furnace 1-10MW/RER U
Residual Oil	USLCI – Residual fuel oil, combusted in industrial boiler/US	Impact Uncertainty: Ecoinvent – heat production, heavy fuel oil, at industrial furnace 1MW/RER
Natural Gas	USCLI – Natural gas, combusted in industrial boiler/US	Impact Uncertainty: Ecoinvent – heat production, natural gas, at boiler >100kW
Petroleum Coke	Converted from coal http://www.epa.gov/climateleadership/documents/emission-factors.pdf	Density: 55 lb/ft3 Impact Uncertainty: Ecoinvent – Heat, at hard coal industrial furnace 1-10MW/RER U
LPG	USLCI – Liquefied petroleum gas, combusted in industrial boiler/US	Impact Uncertainty: Ecoinvent – heat production, natural gas, at boiler >100kW
Electricity	Ecoinvent – Electricity, high voltage {US}| production mix	Impact Uncertainty: Ecoinvent – Electricity, high voltage {US}| production mix
Waste Oil	Treated as zero-impact contributor	
Tire Derived	Treated as zero-impact contributor	
Wood	Treated as zero-impact contributor	
Transportation		
Conveyer	unavailable	Neglected from total (minimal amount used)
Pipeline	Ecoinvent – natural gas, pipeline, long distance/RER	

Truck	Ecoinvent – lorry 3.5-16t, fleet average	
Rail	Ecoinvent – freight rail, diesel, US	
Barge	Ecoinvent – barge tanker/RER	
Ship	Ecoinvent – transoceanic freight ship	
Materials		
Limestone	USLCI – Limestone, at mine/US	Impact Uncertainty: Ecoinvent – Limestone, crushed, washed {CH}| production
Cement Rock	USLCI – Limestone, at mine/US	Similar to limestone
Shale	Ecoinvent – Gravel, crushed {CH}| production	
Clay	Ecoinvent – Clay, at mine/CH	
Sand	Ecoinvent – Silica sand {CH}| production	
Fly Ash	unavailable	Neglected from total (minimal amount used)
Bottom Ash/Slag	unavailable	Neglected from total (minimal amount used)
Blast Furnace Slag	Ecoinvent – Ground granulated blast furnace slag {US}| production	
Iron/Iron Ore	Ecoinvent – Iron mine operation, crude ore, 46% Fe/CH	
Steel Slag	unavailable	Neglected from total (minimal amount used)
Foundry Sand	Ecoinvent – Silica sand {CH}| production	
Blast Sand	Ecoinvent – Silica sand {CH}| production	
Gypsum	Ecoinvent – Gypsum, mineral {CH}| gypsum quarry operation	
Bauxite	Ecoinvent – Bauxite, at mine/GLO	
Calcination	IPCC Good Practice Guidance and Uncertainty Management in National Greenhouse Gas Inventories, 2006 *(96)*	Based on clinker production data

APPENDIX C

Pavement Design Summary

Traffic:

Traffic obtained from city of Boston (https://data.boston.gov/dataset/traffic-related-data), at A st. north of Iron st, which is represents typical local street in Boston, i.e. including two traffic lanes, two parking lanes and two bike lanes.

Site conditions:

- Urban local roadway, one travel lane each direction.
- Traffic loadings: The AADTT two directions is 1600, assuming 50% in the design direction.
- Soil support: AASHTO class is A-2-5, coarse grained soil based on the national soil map developed by Arizona State University. The mean subgrade resilient modulus is 16,000 psi.
- Climate: The project site is in Boston MA.
- Reliability and performance criteria: national default of the program.

The AASHTO Pavement ME program was utilized for the design and M&R.

Analysis Period

Parameter	Value	Units
Design Period	30	years
Analysis Period	50	years

Operational Context

Parameter	Value	Units
AADTT two Directions	1,600	vehicles/day
Number of Total Lanes	2	
Percent trucks in design direction	50%	
AADTT Linear Annual Increase	3%	

117

PCC Pavement-ME M&R Schedule

Year	Activity
New construction	Place 7.5 in. PCC (with 1.25 in diameter dowel) over 4 in. crushed stone material
30	Full depth repair (slab replacement of 0.38% is required in the travel lane)
Salvage at 50	10 years

Reconstruction

Traffic Inputs

| Design period	30
Initial two-way AADTT	1600
Number of lanes in design direction	1
Percent of trucks in design direction (%)	50.0
Percent of trucks in design lane (%)	100.0
Number of trucks over design period	12,579,200

Pavement Structure That Meets Performance & Reliability Requirements

Layer Type	Material Type	Thickness (in)	Dowel Dia. (in)
JPCP-PCC	PCC	7.5	1.25
Granular Base	A-1-a	4	
Subgrade	A-2-5	Semi-infinite	

Distress Prediction & Reliability Summary

| Distress Type | Distress @ Reliability | | Reliability (%) | | Criterion |
	Target	Predicted	Target	Achieved	Satisfied?
Terminal IRI (in./mile)	172.00	125.06	90.00	99.78	Pass
Mean joint faulting (in.)	0.12	0.07	90.00	99.92	Pass
JPCP transverse cracking (percent slabs)	15.00	4.61	90.00	100.00	Pass

Distress Charts
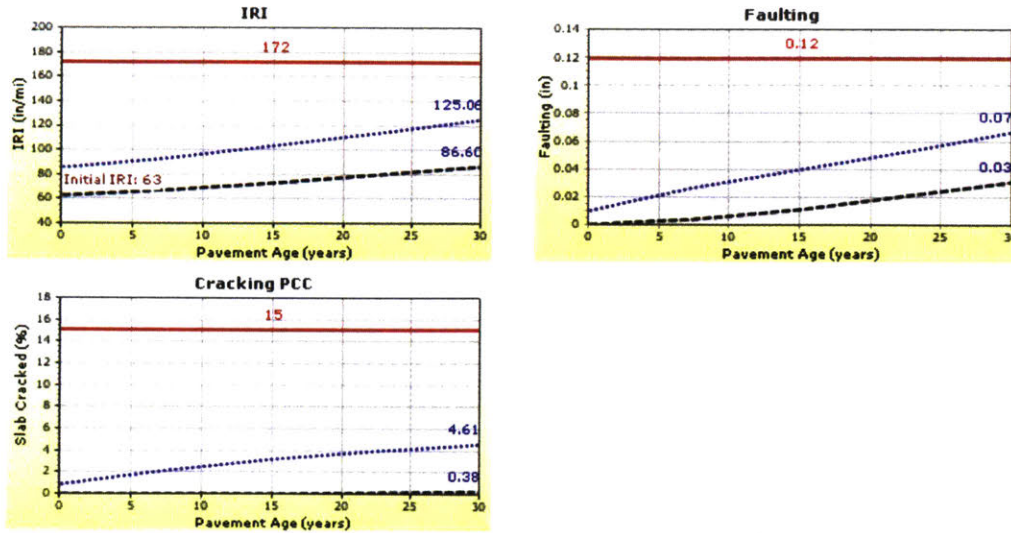
This design passes the threshold criteria over 30 years. At 30 years, there is 4.61% fatigue cracking, 0.07 in faulting and 125.06 in/mile IRI at 90% reliability. Full depth repair and diamond grinding are the most logical M&R treatment at 30 years.

First Rehabilitation -Full Depth Repair & Diamond Grinding (20 yrs)

At 30 years, 0.38% of the slabs (predicted cracked slabs @ 50% reliability) needs to be repaired before diamond grinding is applied. After grinding, the concrete thickness is assumed to be 7.25 in.

Traffic Inputs

Design period (from year 30 to 50)	20
Initial two-way AADTT	3040
Number of lanes in design direction	1
Percent of trucks in design direction (%)	50.0
Percent of trucks in design lane (%)	100.0
Number of trucks over design period	14,268,100

Pavement Structure That Meets Performance & Reliability Requirements

Layer Type	Material Type	Thickness (in)
JPCP-PCC	PCC	7.25*
Granular Base	A-1-a	4
Subgrade	A-2-6	Semi-infinite

*Note: 0.25 inch slab thickness was removed by diamond grinding.

Distress Prediction & Reliability Summary

Distress Type	Distress @ Reliability		Reliability (%)		Criterion
	Target	Predicted	Target	Achieved	Satisfied?
Terminal IRI (in./mile)	172.00	125.33	90.00	99.76	Pass
Mean joint faulting (in.)	0.12	0.07	90.00	99.89	Pass
JPCP transverse cracking (percent slabs)	15.00	8.51	90.00	99.44	Pass

Distress Charts